ADVANCED FUNCTIONAL MATERIALS
www.afm-journal.de

Confinement Effects in Individual Carbon Encapsulated Nonprecious Metal-Based Electrocatalysts

Ling Shen, Jie Ying, Kenneth I. Ozoemena, Christoph Janiak, and Xiao-Yu Yang**

The evolution of cost-effective and reserve-rich nonprecious metals (NPMs) to replace precious metal electrocatalysts is of significant interest in modern electrocatalysis. The confinement effects in NPM-based nanoparticles encapsulated in carbon nanoshells have been considered as an emerging and efficient way to special types of electrocatalysts which facilitate electrocatalytic activity and stability, even under rigorous conditions. This review focuses on the unique individual carbon encapsulation for high-performance design of NPM-based electrocatalysts, outlining all confinement synthesis methods, mechanistic studies on confinement effects, and the emerging practical reactions. It begins first introducing the synthetic methods for NPM-based core@carbon shell electrocatalysts, and then follows clarification of the relationship between the fundamental confinement effects and the performance improvement of carbon shell encapsulating NPM-based electrocatalysts. Further and detailed discussions on the alloying effect, doping effect, and heterojunction effect of the NPM-based core to alter the electronic situation which affects the electrocatalytic performance are subsequently provided. Finally, the review provides a perspective on challenges and opportunities in future research with respect to both in-depth theoretical research and potential design concept of such NPM-based core@carbon shell electrocatalysts.

L. Shen, X.-Y. Yang
State Key Laboratory of Advanced Technology for Materials Synthesis and Processing and School of Materials Science and Engineering
Wuhan University of Technology
No. 122 Luoshi Road, Wuhan 430070, China
E-mail: xyyang@whut.edu.cn

J. Ying
School of Chemical Engineering and Technology
Sun Yat-sen University
Zhuhai 519082, China
E-mail: yingj5@mail.sysu.edu.cn

K. I. Ozoemena
Molecular Sciences Institute
School of Chemistry
University of the Witwatersrand
Private Bag 3, Johannesburg 2050, South Africa

C. Janiak
Institut für Anorganische Chemie und Strukturchemie
Heinrich-Heine-Universität Düsseldorf
40225 Düsseldorf, Germany

X.-Y. Yang
School of Engineering and Applied Sciences
Harvard University
Cambridge, MA 02138, USA
E-mail: xyyang@seas.harvard.edu

The ORCID identification number(s) for the author(s) of this article can be found under https://doi.org/10.1002/adfm.202110851.

DOI: 10.1002/adfm.202110851

1. Introduction

The rising global energy demand and the quest to combat the disastrous environmental impact of fossil-fuel burning have made electrochemical energy conversion, which can convert electricity from renewable sources into storable hydrogen and vice versa, of tremendous interest from scientific and industrial researchers.[1–3] At the same time, new electrocatalysts, that is, electrode materials are needed for necessary improvements in rate, efficiency, and selectivity of the energy conversion.[4–7] Practically, precious metal-based materials (e.g., Pt, Pd, Ru, Ir, Rh, their alloys and compounds) are conventionally state-of-the-art electrocatalysts with excellent electrocatalytic efficiency, and are frequently used in proton exchange membrane fuel cells or water splitting systems.[8–13] Nonetheless, high-cost, limited reserve, and relatively poor long-term stability are the major obstacles of precious metal-based catalysts for large-scale commercialization. For example, Pt is the most efficient catalyst for the cathodic oxygen reduction reaction (ORR) in proton exchange membrane fuel cells.[14–16] However, Pt-based electrocatalysts are responsible for more than 40% of the cost of fuel cells power system.[17–21] In consideration of practical application, such electrocatalysts must be cheap enough to produce and utilize. Therefore, the development of electrocatalysts that comprise only inexpensive, nonprecious metal (NPM) is critical.[22–24] Today's low-cost NPM-based electrocatalysts, however, are inadequate and many important problems should still be resolved for the promise of their practical application, such as fast kinetics, high stability, and durability.[25,26] The grand challenge is to develop advanced NPM-based electrocatalysts with the improved performance needed to enable extensive application of clean energy technologies. As a consequence, the development of NPM-based catalysts with high electrocatalytic activity has recently become a major focus of electrocatalysis research. There are many successful examples on the performance enhancement, such as morphology controlling,[27,28] facet adjusting,[29,30] junction engineering,[31,32] and single-atom capturing.[33,34] To further improve the stability, durability, and utilization efficiency of metals, various types of nanoarchitectures and nanomaterials have been employed as catalyst supports.[35–38]

For practical application and structural stability, carbon materials are most widely used as electrocatalytic supports

for nanometal dispersions with a view to both interaction enhancement and cost reduction for a long time.[39–45] Activated carbons with high surface area have been first exploited as carbon supports for metal electrocatalysts in the middle 1960s and since then served as support materials for precious metals, e.g., Pt/C commercial catalysts.[46] In the late 1990s, CNTs with remarkable electrochemical properties were developed as supports, and numerous dispersed metals exhibited largely enhanced electroactivities.[47,48] Since the early 2000s, the mesoporous carbons, carbon nanofibers, and graphene were subsequently developed for high-performance design of nanometallic electrocatalysts.[49–52] In the early 2010s, metal-organic framework (MOF) derived porous carbons were utilized to obtain highly stable metallic electrocatalysts.[53–55] For confined synthesis with carbon materials, that is inside their pore systems, it permits size control, facet adjustment, and morphology-controlled fabrication of nanometals. The beauty of such confined synthesis lies in the fact that strong enough interactions of nanometals with the porous support and separation within the pore system can prevent nano-aggregation. Advantageous features of nanoarchitectures allow for high accessibility and corresponding confined catalysis by creating stable, finely dispersed nanometals with a high catalytic activity.[56,57] Three main carbon encapsulation technologies of nanounits (adsorption, covalent binding, and entrapment) have been recently used to enhance stability and reusability of the metastable nano/atomic sites for further applications. Note that they share a porous support with high surface area, tunable porosity, and good resistance to chemical attack. For electrocatalysis, the ions H^+ and OH^- in corresponding acidic and basic conditions penetrate almost all porous structures from macro-, meso-, to microporosity to the surface of the NPM-based electrocatalytic centers. This direct contact would, however, result in a greatly decreased activity and stability of NPM-based electrocatalytic centers.

In 2011, Science magazine reported a breakthrough on iron and cobalt electrocatalysts coated with a very thin carbon layer, which resulted in an excellent combination of high activity with remarkable stability and specific four-electron selectivity for ORR.[58] Soon afterwards, this elegant idea inspired an individual encapsulation approach to fabricate a carbon nanoshell on numerous NPM-based cores with various metal elements (mainly including Mn, Fe, Co, Ni, Cu, Zn, Mo, W) and nonmetal elements (mainly including C, N, O, P, S, Se) as alloying or doping elements, which has been considered as an emerging and efficient way (so-called individual carbon encapsulation) to improve catalyst stability and functionality for enhanced adaption in practical electrocatalysis applications, mainly including hydrogen evolution reaction (HER), ORR and oxygen evolution reaction (OER) (**Figure 1** and **Table 1**).[59–69] The advantageous features include that a carbon nanoshell can protect the NPM-based cores from the reaction with exterior H^+ and OH^-, and prevent the NPM-based cores from aggregation. Although NPM-based cores are introduced into the carbon shell which forms a physical separation from the electrolyte, these cores and the carbon shells can interact to effectively adjust the electronic situation of the carbon shell surface, which facilitates the catalytic reaction. This individual encapsulation within a nanoscale carbon shell is often considered as a complete confinement and the corresponding confinement invoked to facilitate the directed catalysis on the surface of the carbon shell via a synergistic effect of the core and the shell.[70,71]

Affected by the NPM-based core, the outside carbon shell is frequently considered as the main and the only active sites in this core–shell structural electrocatalysts. However, it exists some controversy whether the shell acts as the only catalytic sites, or both the core and the shell are the catalytic sites. There is no denying that a unique effect of nanoconfinement via individual carbon encapsulation for electrocatalysts is the modulation of the electronic structure of the outer carbon layer, which provides a combination of the protection and stable dispersion of NPM-based cores, acceleration of chemical reactions, enhancement or alteration of selectivity and resultant promotion of electrochemical performance.[72,73]

The search for a replacement of precious-metal electrocatalysts made the NPM-based core@carbon shell electrocatalysts undergo a rapid development in the past 10 years (Figure 1B). The related NPM-based electrocatalysts with different cores such as various alloys, doping, and nanosized composition heterojunctions were also rapidly developed in electrocatalysis. Owing to the strong scientific interest and practical importance of this field, a series of recent reviews on NPM-based electrocatalysts have been published. Each of these reviews addresses mainly structural aspects and their corresponding properties and applications, including individual electrocatalytic reaction (HER, ORR, or OER) and structural design.[74–77] Note that the discussion of confinement effect in previous review mainly emphasized carbon shell (such as layer number and doping functionalization) and alloying core (binary-/ternary-alloying and related metallic compounds). With further study of the mechanism of confinement effect, some important viewpoints and corresponding questions need discussion and clarification, for example, difference of active sites in the cores and the shells and corresponding central role, and the role of carbon shell thickness and unusual enhancement of catalytic activity in the presence of relative thick carbon shell. Notably, these viewpoints and corresponding questions are not deeply discussed in previous reviews. With appearance of atom-level nanotechniques, precise doping and oriented heterojunction have been developed for adjusting metal-based core. Compared to the previous review, our review discusses doping effect and heterojunction effect of metal-based core, which are also rarely further discussed. In this regard, a review focuses on the unique individual carbon encapsulation for high-performance design of NPM-based electrocatalysts, outlining all confinement synthesis methods, mechanistic studies on confinement effects and the emerging practical reactions, therefore seems warranted. Our review thoroughly analyses in depth confinement effects in shell part (pure carbon, mono-doping, multiple-doping, multiple layer) and core part (alloying effect, doping effect, and heterojunction effect), and their core–shell interactions. Especially, we propose and try to clarify the viewpoints above-mentioned for these related electrocatalyst design.

This review is aimed at fully illuminating the recent research progress on the enhancement of the electrocatalytic activity and stability for carbon confined NPM-based core@shell electrocatalysts via the combination of theoretical

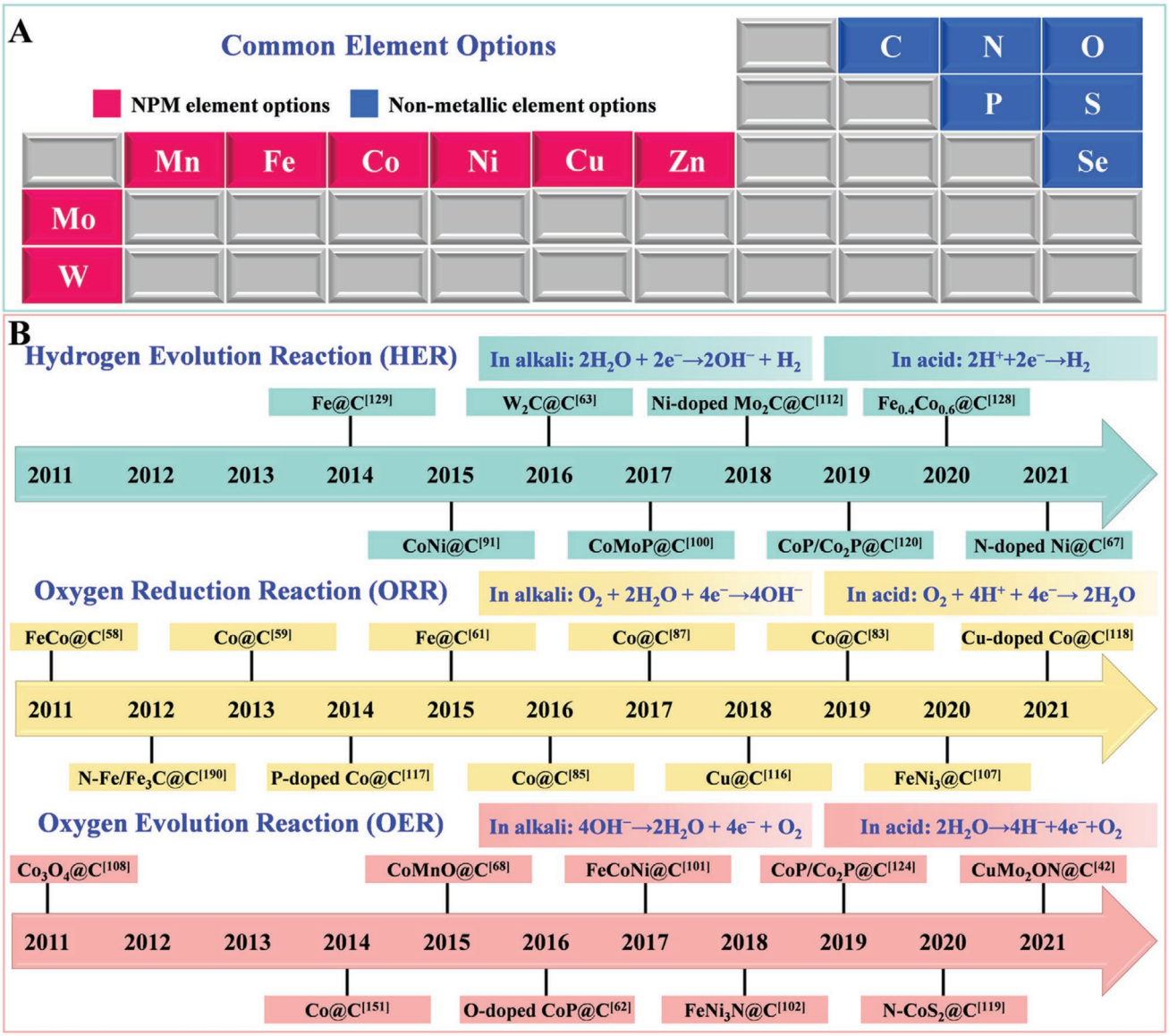

Figure 1. A) The elements that are usually used in NPM-based core@carbon shell electrocatalysts in this review. B) Reaction equations of HER, ORR, and OER and the timeline of representative NPM-based core@carbon shell electrocatalysts (labeled as NPM-based core@C) in the last decade for HER, ORR, and OER, respectively. The corresponding reference of the electrocatalyst is marked in square brackets in the upper right corner.

calculation and experimental results. It is organized by first introducing the synthetic methods for NPM-based core@carbon shell electrocatalysts (Section 2). Then follows clarification of the relationship between the fundamental confinement effect and the performance improvement of carbon shell encapsulating NPM-based electrocatalysts (Section 3). On this basis, further and detailed discussions on the alloying effect (Section 4.1), doping effect (Section 4.2), and heterojunction effect (Section 4.3) of the NPM-based core to alter the electronic situation which affect the electrocatalytic performance have been provided (**Figure 2**). Finally, the review provides a perspective (Section 5) on challenges and opportunities in future research with respect to both in-depth theoretical research and potential design concept of such NPM-based core@carbon shell electrocatalysts.

2. Confinement Synthesis

The synthesis of individual carbon shell-confined NPM-based cores can be categorized into three basic methods: i) solid-phase synthesis, ii) liquid-phase synthesis, and iii) gas-phase synthesis (**Figure 3**).

2.1. Solid-Phase Synthesis

The typical solid-phase reaction for the synthesis of NPM-based core@carbon shell electrocatalysts is mostly conducted by external force for mixing (mainly including grinding or ball-milling) followed by pyrolysis. The benefits of this synthesis route are low cost, and possible scale-up for production.

Table 1. Comparison of performance for various NPM-based core@carbon shell electrocatalysts with different categories.

Catalysts	Electrolyte	Catalytic activity[a)]	Stability times (test condition)/cycles[b)]	Refs.
Single core@carbon shell for HER				
Fe@carbon shell/SWCNTs[c)]	0.5 M H_2SO_4	η@10 = 77, TS = 40	18 h (–0.135 V)/1000 cycles	[78]
Co@B,N-codoped carbon shell	0.5 M H_2SO_4	η@10 = 96, TS = 63.7	10 h (–0.2 V)/2000 cycles	[79]
	1.0 M KOH	η@10 = 183, TS = 73.2	10 h (–0.25 V)/2000 cycles	[79]
Co@Co,N-codoped carbon shell	0.1 M KOH	η@10 = 314, TS = 59	20 000 s (–0.3 V)/2000 cycles	[80]
Ni@graphene shell	1.0 M KOH	η@10 = 240, TS = 120	10 h (–0.2 V)	[64]
Single core@carbon shell for ORR				
Co@S,N-codoped carbon shell	0.1 M $HClO_4$	OP = 0.852, HP = 0.68	10 000 cycles	[81]
Fe@N-doped carbon shell/C_2N[d)]	0.1 M KOH	OP = 1.015, HP = 0.876	100 000 cycles	[82]
Co@graphene shell/carbon black	0.1 M KOH	HP = 0.8	5000 cycles	[83]
Co@carbon shell/N-doped graphene nanoribbons	0.1 M KOH	OP = 0.91, HP = 0.83	3000 cycles	[84]
Co@N-doped carbon shell/NWCs[e)]	0.1 M KOH	OP = 0.939, HP = 0.83	250 min (0.75 V)/6000 cycles	[85]
Co@N-doped carbon shell	0.1 M KOH	OP = 0.98, HP = 0.84	100 000 s (0.6 V)/3000 cycles	[86]
Co@N-doped carbon shell/N-doped carbon sheets	0.1 M KOH	HP = 0.85	20 000 s (0.75 V)	[87]
Co@S,N-codoped carbon shell	0.1 M KOH	OP = 0.990, HP = 0.831	10 000 cycles	[81]
Co@Co,N-codoped carbon shell	0.1 M KOH	OP = 1.02, HP = 0.879	2000 cycles	[80]
Cu@N-doped carbon shell	0.1 M KOH	OP = 0.94, HP = 0.83	500 min (0.7 V)/3000 cycles	[60]
Single core@carbon shell for OER				
Co@N-doped carbon shell	0.1 M KOH	η@10 = 390, TS = 110	10 h (10 mA cm^{-2})	[86]
Co@carbon shell embedded in porous N-doped CNFs[f)]	1.0 M KOH	η@10 = 285, TS = 73	12 h (1.54 V)/5000 cycles	[88]
Ni@graphene shell	1.0 M KOH	η@10 = 370, TS = 66	12 h (10 mA cm^{-2})	[64]
Alloy core@carbon shell for HER				
FeCo@N-doped graphene shell	0.5 M H_2SO_4	η@10 = 262, TS = 74	11 h (–0.3 V)/10 000 cycles	[89]
FeP@N,P-codoped carbon shell	0.5 M H_2SO_4	η@10 = 130, TS = 67	20 h (–0.14 V)/5000 cycles	[90]
CoNi@N-doped graphene shell	0.1 M H_2SO_4	η@10 = 224, TS = 104	24 h (20 mA cm^{-2})/1000 cycles	[91]
Co_2P@N,P-codoped graphene shell	0.5 M H_2SO_4	η@10 = 103, TS = 58	30 h (–0.100 V)/10 000 cycles	[92]
CoS@graphene shell/N,S-codoped RGO[g)]	0.5 M H_2SO_4	η@10 = 74, TS = 56	10 h (–0.12 V)/500 cycles	[65]
NiMo@N-doped graphene shell/3D N-doped graphene	0.5 M H_2SO_4	η@10 = 80, TS = 54	25 h (–0.2 V)/2000 cycles	[93]
Ni_2P@P-doped carbon shell/P-doped graphene	0.5 M H_2SO_4	η@10 = 110, TS = 58.6	25 h (10 mA cm^{-2})/5000 cycles	[94]
Cu_3P@N,P-codoped carbon shell	0.5 M H_2SO_4	η@10 = 89, TS = 76	3000 cycles	[95]
Mo_2C@N-doped carbon shell	0.5 M H_2SO_4	η@10 = 124, TS = 60	80 h (–0.07 V)	[96]
Mo_2C@N-doped graphene shell	0.5 M H_2SO_4	η@10 = 78, TS = 41	12 h (–0.078 V)/2000 cycles	[97]
MoP@N-doped carbon shell	0.5 M H_2SO_4	η@10 = 115, TS = 65	100 h (–0.12 V)/10 000 cycles	[98]
WP@N-doped carbon shell	0.5 M H_2SO_4	η@10 = 102, TS = 58	96 h (–0.08 V)/6000 cycles	[99]
CoMoP@N-doped carbon shell	0.5 M H_2SO_4	η@10 = 41, TS = 49.73	24 h (–0.12 V)/10 000 cycles	[100]
FeP@N,P-codoped carbon shell	1.0 M PBS[h)]	η@10 = 386, TS = 136	10 h (–0.4 V)	[90]
Mo_2C@N-doped carbon shell	0.1 M PBS	η@10 = 156	15 h (–0.096 V)	[96]
MoP@N-doped carbon shell	1.0 M PBS	η@10 = 136, TS = 71	20 h (–0.15 V)	[98]
WP@N-doped carbon shell	1.0 M PBS	η@10 = 196	20 h (–0.2 V)	[99]
FeP@N,P-codoped carbon shell	1.0 M KOH	η@10 = 214, TS = 82	10 h (–0.22 V)	[90]
FeCoNi@N-doped graphene shell	1.0 M KOH	η@10 = 325, TS = 60	10 000 cycles	[101]
$FeNi_3N$@N-doped carbon shell/N-doped graphene	1.0 M KOH	η@10 = 94, TS = 90	10 h (–0.12 V)/2000 cycles	[102]
CoS@graphene shell/N,S-codoped RGO	1.0 M KOH	η@10 = 118, TS = 63	10 h (–0.17 V)/500 cycles	[65]
CoMnO@N-doped carbon shell	1.0 M KOH	η@20 = 71, TS = 152	32 h (–0.2 V)	[68]
CoMoP@N-doped carbon shell	1.0 M KOH	η@10 = 81, TS = 55.53	24 h (–0.12 V)/10 000 cycles	[100]
Ni_2P@P-doped carbon shell/P-doped graphene	1.0 M KOH	η@10 = 150, TS = 79.4	25 h (10 mA cm^{-2})/5000 cycles	[94]

Table 1. Continued.

Catalysts	Electrolyte	Catalytic activity[a)]	Stability times (test condition)/cycles[b)]	Refs.
Mo_2C@N-doped carbon shell	1.0 M KOH	η@10 = 60	15 h (–0.063 V)	[96]
MoP@N-doped carbon shell	1.0 M KOH	η@10 = 80, TS = 59	20 h (–0.1 V)	[98]
WP@N-doped carbon shell	1.0 M KOH	η@10 = 150	20 h (–0.15 V)	[99]
Alloy core@carbon shell for ORR				
Fe_2N@N-doped carbon shell	1.0 M $HClO_4$	OP = 0.82, HP = 0.71	10.5 h (0.5 V)	[103]
FeCo@carbon shell embedded in SWCNTs	0.1 M KOH	HP = 0.796	7.5 h (0.796 V)	[104]
FeCo@N-doped carbon shell/N-doped graphene	0.1 M KOH	OP = 0.9, HP = 0.86	500 min (0.8 V)/20 000 cycles	[105]
FeNi@N-doped carbon shell/N-doped graphene	0.1 M KOH	OP = 1.06, HP = 0.86	10 h (0.8 V)/20 000 cycles	[106]
$FeNi_3$@N-doped graphene shell/3D N-doped graphene	0.1 M KOH	OP = 0.93, HP = 0.80	20 000 s (0.8 V)	[107]
Fe_2N@N-doped carbon shell	0.1 M KOH	OP = 1.02, HP = 0.93	9 h (0.5 V)	[103]
Co_3O_4@N-doped RGO	0.1 M KOH	HP = 0.83, TS = 42	25 000 s (0.7 V)	[108]
Cu_3P@N,P-codoped carbon shell	0.1 M KOH	HP = 0.78	8 h (0.6 V)/3000 cycles	[95]
Alloy core@carbon shell for OER				
FeCo@carbon shell embedded in SWCNTs	1.0 M KOH	η@10 = 253, TS = 44	50 h (1.527 V)	[104]
FeCo@N-doped carbon shell/N-doped graphene	0.1 M KOH	η@10 = 440, TS = 90	500 min (1.6 V)	[105]
$(Fe_4Co_1)P_2O_7$@N-doped carbon shell	1.0 M KOH	η@10 = 341, TS = 34.9	80 h (20 mA cm^{-2})/5000 cycles	[109]
FeNi@N-doped carbon shell/N-doped graphene	0.1 M KOH	η@10 = 325, TS = 60.6	10 h (1.55 V)/1000 cycles	[106]
$FeNi_3$@N-doped graphene shell/3D N-doped graphene	0.1 M KOH	η@10 = 310, TS = 85.8	30 000 s (10 mA cm^{-2})	[107]
	1.0 M KOH	η@10 = 239, TS = 44.8	36 000 s (10 mA cm^{-2})	[107]
FeNi@N-doped graphene shell	1.0 M KOH	η@10 = 280, TS = 70	24 h (10 mA cm^{-2})/1000 cycles	[110]
FeNi@N-doped graphene shell	1.0 M NaOH	η@10 = 280, TS = 70	10 000 cycles	[111]
$FeNi_3N$@N-doped carbon shell/N-doped graphene	1.0 M KOH	η@10 = 270, TS = 54	10 h (1.51 V)/2000 cycles	[102]
Co_3O_4@N-doped RGO	1.0 M KOH	η@10 = 310, TS = 67	1500 cycles	[108]
CoMnO@N-doped carbon shell	1.0 M KOH	η@308 = 420, TS = 97	40 h (1.55 V)	[68]
Doping core@carbon shell for HER				
Ni-doped Mo_2C@N-doped carbon shell	0.5 M H_2SO_4	η@10 = 72, TS = 65.6	24 h (–0.072 V)/2000 cycles	[112]
O-doped MoP@RGO	0.5 M H_2SO_4	η@20 = 118, TS = 58	5000 cycles	[62]
Ni-doped MoP@N-doped carbon shell	0.5 M H_2SO_4	η@10 = 102, TS = 58.1	10 mA cm^{-2}@10 h	[113]
	1.0 M PBS	η@10 = 222, TS = 160.4	10 mA cm^{-2}@10 h	[113]
N-doped Ni@N-doped carbon shell	1.0 M KOH	η@10 = 61, TS = 71	12 h (20 mA cm^{-2})	[114]
N-doped Ni@N-doped carbon shell	1.0 M KOH	η@10 = 28, TS = 39	40 h (–0.025 V)	[67]
	1.0 M KOH seawater	η@10 = 23, TS = 41	40 h (–0.025 V)	[67]
Mo-doped Ni@N-doped carbon shell/SWCNTs	1.0 M KOH	η@10 = 130, TS = 128	20 h (0.17 V)/5000 cycles	[115]
O-doped MoP@RGO	1.0 M KOH	η@20 = 93	5000 cycles	[62]
Ni-doped MoP@N-doped carbon shell	1.0 M KOH	η@10 = 162, TS = 102.6	10 mA cm^{-2}@10 h	[113]
Doping core@carbon shell for ORR				
N-doped Cu@Fe,N-codoped carbon shell	0.5 M H_2SO_4	OP = 0.88, HP = 0.761	20 000 s	[116]
P-doped Co@carbon shell/carbon black	0.1 M KOH	HP = 0.8	5000 cycles	[117]
Cu-doped Co@Cu,Co,N-multidoped carbon shell	0.1 M KOH	OP = 0.98, HP = 0.88	55 h (0.75 V)/5000 cycles	[118]
N-doped Cu@Fe,N-codoped carbon shell	0.1 M KOH	OP = 1.01, HP = 0.892	20 000 s	[116]
Doping core@carbon shell for OER				
O-doped CoP@RGO	1.0 M KOH	η@10 = 280, TS = 75	5000 cycles	[62]
N-doped CoS_2@N-doped graphene shell	1.0 M KOH	η@10 = 205, TS = 65	9.5 h (10 mA cm^{-2})/1000 cycles	[119]
Mo-doped Ni@N-doped carbon shell/SWCNTs	1.0 M KOH	η@10 = 255, TS = 54	20 h (1.52 V)/5000 cycles	[115]
Heterojunction core@carbon shell for HER				
CoP/Co_2P@N-doped carbon shell	0.5 M H_2SO_4	η@10 = 126, TS = 79	24 h (–0.2 V)/1000 cycles	[120]

Table 1. Continued.

Catalysts	Electrolyte	Catalytic activity[a)]	Stability times (test condition)/cycles[b)]	Refs.
Ni/Ni_2P@carbon shell	0.5 M H_2SO_4	η@10 = 149, TS = 61.2	8 h (–0.15 V)/1000 cycles	[121]
MoP/Mo_2C@N-doped carbon shell	0.5 M H_2SO_4	η@10 = 89, TS = 45	14 h (–0.075 V)/1000 cycles	[122]
CoP/Co_2P@N-doped carbon shell	1.0 M PBS	η@10 = 459	20 h (–0.5 V)	[120]
MoP/Mo_2C@N-doped carbon shell	1.0 M PBS	η@10 = 136, TS = 93	14 h (–0.13 V)/1000 cycles	[122]
Co/Co_3ZnC@carbon shell embedded in NCCP[i)]	1.0 M KOH	η@10 = 188, TS = 108	10 h (–0.2 V)/1000 cycles	[123]
CoP/Co_2P@N-doped carbon shell	1.0 M KOH	η@10 = 198, TS = 82	24 h (–0.3 V)/1000 cycles	[120]
CoP/Co_2P@P-doped carbon shell/P-doped graphene	1.0 M KOH	η@10 = 39, TS = 59	5000 cycles	[124]
MoP/Mo_2C@N-doped carbon shell	1.0 M KOH	η@10 = 75, TS = 58	14 h (–0.060 V)/1000 cycles	[122]
Heterojunction core@carbon shell for ORR				
Fe/Fe_5C_2@graphene/N-doped graphene nanosheets	0.1 M KOH	OP = 0.98, HP = 0.86	15 h (0.6 V)	[125]
Co/Co_3ZnC@N-doped graphene shell	0.1 M KOH	OP = 0.912, HP = 0.725	40 000 s (0.45 V)/5000 cycles	[69]
Co_2P/Co_xN@N-doped carbon shell/N-doped graphene	0.1 M KOH	OP = 0.93, TS = 56	2000 cycles	[126]
Heterojunction core@carbon shell for OER				
Co/Co_3ZnC@N-doped graphene shell	1.0 M KOH	η@10 = 366, TS = 81	5000 cycles	[69]
Co/Co_3ZnC@carbon shell embedded in NCCP	1.0 M KOH	η@10 = 295, TS = 70	10 h (1.53 V)/1000 cycles	[123]
CoP/Co_2P@P-doped carbon shell/P-doped graphene	1.0 M KOH	η@20 = 272, TS = 66	5000 cycles	[124]

[a)]In the column of catalytic activity: $\eta@j$ = overpotential (mV) at a given current density (mA cm^{-2}), TS = Tafel slope (mV dec^{-1}), OP = onset potential (V), HP = half-wave potential (V); [b)]Times (test condition)/cycles: The current density can be kept stable for a period of time under the given test conditions/the LSV curves can be almost unchanged or slightly become inferior after a given number of CV cycles; [c)]SWCNTs: single-walled carbon nanotube; [d)]C_2N: nitrogenated holey 2D network; [e)]NWCs: N-doped wrinkled carbon nanosheets; [f)]CNFs: carbon nanofibers; [g)]RGO: reduced graphene oxide; [h)]PBS: phosphate buffer solution (pH = 7); [i)]NCCP: N-doped carbon nanotube-grafted carbon polyhedral.

A manual grinding-pyrolysis solid-phase synthesis method is used to prepare Cu-layer-decorated Co nanoparticles which are confined in a Cu–N_x and Co–N_x codoped graphene nanoshell (Figure 3A).[118] For this specific example, a stoichiometric ratio of metal precursors ($Co(NO_3)_2 \cdot 6H_2O$ and $Cu(NO_3)_2 \cdot 3H_2O$) were mixed with dicyandiamide used as both carbon and nitrogen source by grinding. Then the paste-like precursor was annealed at 800 °C for 2.5 h in Ar atmosphere. Subsequently, acid leaching was conducted to remove excessive metallic debris in the product. The product was washed by water and ethanol, followed by a drying process. The size of Co nanoparticles partly decorated with Cu layer was between 20 and 50 nm, coated with a 0.5–2 nm thick carbon shell. In order to promote the uniform mixing of the raw materials, ball-milling can replace manual grinding. For example, after ball-milling, the mixture of C_3N_4, $Fe(acac)_3$ and $Co(acac)_2$ was pyrolyzed under N_2 atmosphere at 800 °C for 4 h in a tube furnace (Figure 3B).[105] The final black product was treated in acid solution, washed with water, and dried. In the product, many small black spheres with the size ranging from 5 to 20 nm consisted of the FeCo alloy nanoparticle core and a few layers of the carbon shell.

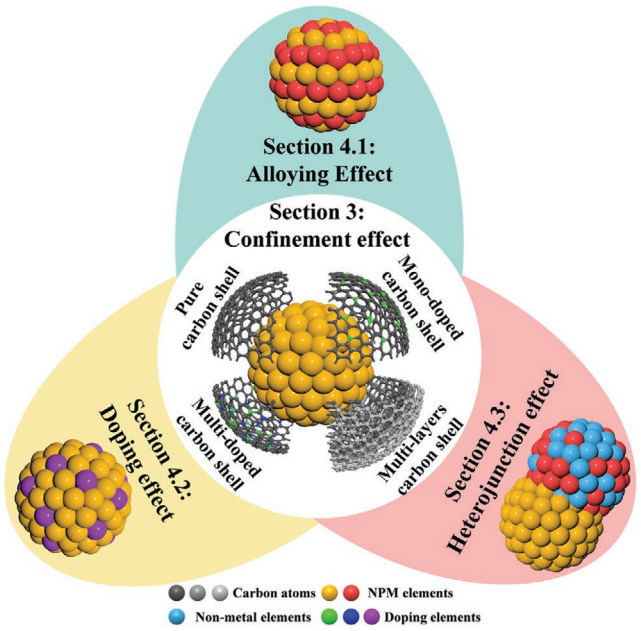

Figure 2. Scheme showing the four effects in NPM-based core@carbon shell electrocatalysts.

Due to the feasibility and handleability of this solid-phase reaction strategy, many other NPM-based core@carbon shell electrocatalysts were also prepared to improve the electrocatalytic performance.[96,112,125] Without doubt, the solid-phase reaction could easily be utilized for large-scale synthesis of NPM-based materials by adjusting the raw materials proportion and equipment size. Recently, a series of NPM phosphides encapsulated in an N-doped carbon shell (NC) were reported by Pu et al. via the solid-phase reaction and post-thermal decomposition, such as WP@NC, MoP @NC, Co_2P@NC, CoP@NC, Ni_2P@NC, $Ni_{12}P_5$@NC, Fe_2P@NC, and FeP@NC.[98,99,127] It has to be pointed out that the size uniformity of the NPM-based core and the thickness uniformity of the carbon shell were more difficult to control.

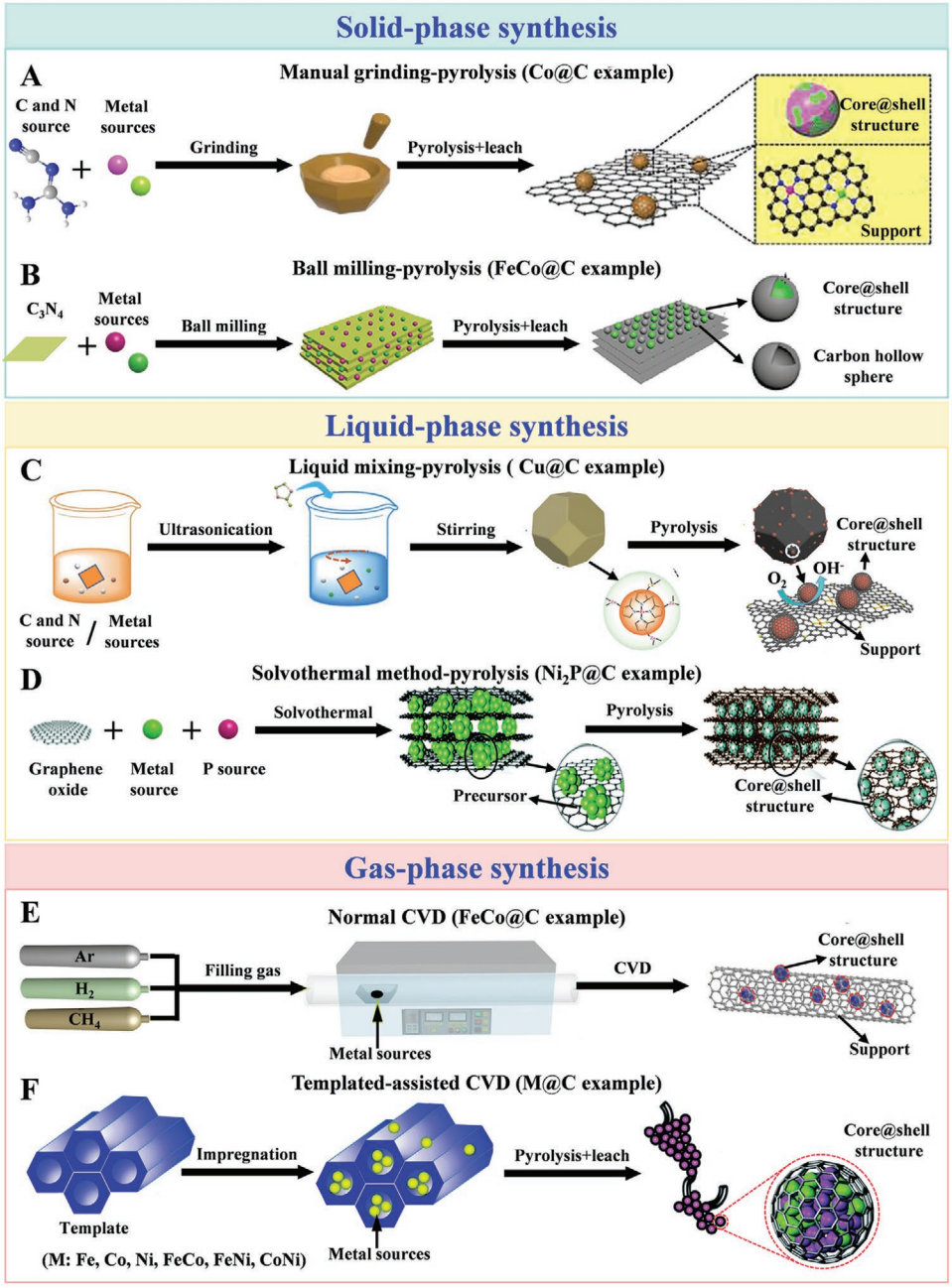

Figure 3. Schematic illustration of the different synthetic methods for NPM-based core@carbon shell electrocatalysts (label as NPM-based core@C): A,B) solid-phase synthesis, C,D) liquid-phase synthesis, E,F) gas-phase synthesis. A) Reproduced with permission.[118] Copyright 2021, Wiley-VCH. B) Reproduced with permission.[105] Copyright 2017, Springer Nature. C) Reproduced with permission.[116] Copyright 2018, Wiley-VCH. D) Reproduced with permission.[94] Copyright 2018, Royal Society of Chemistry. E) Reproduced with permission.[104] Copyright 2020, Royal Society of Chemistry. F) Reproduced with permission.[111] Copyright 2016, Royal Society of Chemistry.

2.2. Liquid-Phase Synthesis

To achieve a better homogeneity or coordination of the precursors, a liquid-phase reaction has widely been used. One universal way for a liquid-phase reaction is to mix solvent, metal sources, carbon sources, and/or doping chemicals together, and to prepare homogeneous solid precursors by stirring, drying, evaporating, freeze-drying, and so on. Finally, the precursors can be treated by pyrolysis under protective/reductive gas. Khani et al. described that various stoichiometric ratios of metal salts were mixed in water with citric acid under stirring at 120 °C until forming a gel followed by drying at 120 °C overnight.[128] Then, the dried precursors were ground and heated in a tube furnace at 800 °C for 6 h under Ar gas. The final products revealed a graphitic-shell encapsulated metal structure involving Fe, Co, Ni, FeCo, FeNi, CoNi, or FeCoNi. In addition,

graphene oxide (GO) sheets, surfactants (polyvinylpyrrolidone, P123, Brij 58) and templates (mesoporous silica (SBA-15), polystyrene particles, SiO_2@resorcinol-formaldehyde spheres) were selectively added into the liquid-phase synthesis process to get the desired structures.[81,85,89,110,124,129,130] Recently, MOF-derived materials received high attention.[131,132] MOFs feature high specific surface areas, abundant pores, controlled sizes, and diverse combinations of metal ions and ligands. Using MOFs or the subgroup of zeolitic imidazolate frameworks (ZIFs) as precursors different carbon-shell encapsulated NPM-based electrocatalysts were obtained by pyrolysis.[121,133] For instance, Wang et al. reported a Fe,Cu-codoped ZIF-8-derived carbon framework with Cu nanoparticles encapsulated in a graphitic carbon shell by liquid-phase synthesis (Figure 3C).[116] Briefly, Fe,Cu-codoped ZIF-8 was first prepared by ultrasound from the methanol solution containing $Zn(NO_3)_2 \cdot 6H_2O$, $Fe(NO_3)_3 \cdot 9H_2O$ and cleaned copper foil for 1 h. Subsequently, the final product was obtained by pyrolyzing the as-prepared ZIF precursor at 900 °C for 3 h under Ar atmosphere. Notably, biomass containing abundant heteroatoms were often converted into functionalized carbon materials.[134,135] In consideration of promoting the synthesis with environmentally friendly, nontoxic, and economical features, the biomass worked as carbon or doping sources in the liquid-phase reaction to get pyrolytic precursors.[90,136]

Hydrothermal or solvothermal reaction involves heating the system to a temperature near or above the boiling point of the solvent in a sealed container (e.g., autoclave) to form an autogenous pressure environment in the container to obtain the required materials. Hydrothermal or solvothermal conditions offer higher diffusivity, lower viscosity, better mass transport, and higher solubility of starting materials, and thus enhance the reaction kinetics. Moreover, introducing additives (e.g., surfactants, dopants) synchronously facilitates the size and morphology control, and also doping modifications without other pretreatment or posttreatment. Miao et al. reported Ni_2P nanoparticles (≈20 nm) encapsulated in two to five layers of a P-doped carbon shell anchored on a graphene network (Figure 3D).[94] In a typical experiment, $NiCl_2 \cdot 6H_2O$, $NaH_2PO_2 \cdot H_2O$, and GO solution were homogeneously dispersed in a mixed solution of water and N,N-dimethylformamide. Then, the autoclave containing the above mixture was maintained at 160 °C for 16 h. Finally, the dried black precipitate was annealed under a mixed Ar/H_2 atmosphere at 500 °C for 4 h. Likewise, Deng et al. synthesized graphene shell encapsulated CoNi alloy nanoparticles by solvothermal method.[91] Originally, an aqueous solution of $Co(NO_3)_2$, $Ni(NO_3)_2$ and tetrasodium ethylenediaminetetraacetate (Na_4EDTA) mixed in methanol was heated at 200 °C for 24 h to gain the EDTA–CoNi. Subsequently, EDTA–CoNi was annealed at 475 °C in Ar atmosphere. The C and N atoms in $EDTA^{4-}$ which was coordinated to the metal ions, the generated CN_x species transferred into graphene shells around CoNi nanoparticles during the thermal decomposition process. The final graphene shells consisted of no more than three layers and the size of the nanoparticles was 4–7 nm. The high temperature and pressure environment during the hydrothermal or solvothermal reaction cannot only improve the solubility of the reactants, but also improves the reactivity of the reactants. So, it facilitated the formation of more uniform NPM-based cores in most works.[100,137,138]

2.3. Gas-Phase Synthesis

Apart from the aforementioned methods, chemical vapor deposition (CVD), as a versatile and popular gas-phase synthesis technique for nanomaterials, is used as well. Conventional CVD uses chemical reactions from gaseous reactants within an activated environment, to deposit a solid product. Although CVD is a complex chemical system, it has been a popular synthetic technique on the basis of some advantages, such as good reproducibility, controllability, and flexibility of the reactants and reaction process, good coverage of the shell and thin films or shells on different shapes.[139–141] In this respect, FeCo alloy nanoparticles@single-layer carbon shell, loaded on single-walled CNTs, were reported by Xie et al. via an aerosol-assisted floating catalyst CVD (Figure 3E).[104] A mist of ferrocene, cobaltocene, and thiophene was introduced into the equipment with H_2 gas and Ar gas. After heating to 800 °C, CH_4 gas was introduced and reacted for 0.5 h. Later, the temperature was raised to 1150 °C to obtain FeCo nanoparticles. Finally, the product was separated through a stainless steel mesh located at the cool zone. Moreover, hot filament CVD (HF-CVD) was also used to prepare NPM-based core@carbon shell electrocatalysts. For example, Fan et al. utilized HF-CVD to get Fe_3C, Co_3C, and Ni_3C nanoparticles encased in a carbon shell decorated on vertically aligned graphene nanoribbons (VA-GNRs).[142] In general, VA-GNRs were first obtained from vertically aligned CNTs by HF-CVD. Subsequently, a layer of metal deposited on the tips of the prepared VA-GNRs underwent the same HF-CVD at 675 °C in the CVD furnace chamber. Finally, M_3C-GNRs (M: Fe, Co, Ni) products were peeled off from the Si substrate. The size of most M_3C nanoparticles was less than 20 nm. The novel structure exposed more active sites and was beneficial to the diffusion of the electrolyte.

Furthermore, Bao et al. synthesized a series of ultrathin carbon-shell encapsulating NPM nanoparticle (Fe, Co, Ni or their bimetallic alloy) catalysts by a template-assisted CVD method, with for example SBA-15 as a template during CVD (Figure 3F).[111,143] In general, the metal salt solution was filled into the SBA-15 template by wet impregnation. Then, the mixtures were treated by CVD at 700 °C under 50% H_2/Ar, followed by introducing CH_3CN as C and N source with Ar carrier gas into the CVD furnace. Finally, SBA-15 was removed by aqueous HF solution to obtain uniform nanoparticles with an average diameter of 6–10 nm confined in a single graphene layer. It was attributed to SBA-15 with its channel structure, that the ultrafine metal nanoparticles and ultrathin carbon shells were almost synchronously obtained in the channels. CVD could control the crystal structure, surface morphology, and the graphitization degree of carbon components in the products. Especially, in the synthesis of a core–shell structure, the uniformity of nanoparticles, the thickness of the shell can be well controlled to reach the ideal target by adjusting the parameters and the feeding.[115,144,145] CVD remains one of the reproducible and fast synthetic techniques to get NPM-based core@carbon shell electrocatalysts.

3. Confinement Effects of Carbon Shells

Inspired from living systems, the study of confinement effects is meaningful for catalysis. In order to have a holistic

understanding of confinement effects, physical and chemical properties of the core–shell structure should be considered in parallel.[73,146–149] Through the aforementioned confinement synthesis, the shape of the NPM-based core is often distinctly affected within the carbon shell by the restricted inner nanospace. This physical separation could strongly stabilize the NPM-based core. For instance, Wang et al. prepared a core–shell material consisting of a graphene shell with the thickness of 1–2 nm encapsulating Cu nanoparticles by CVD.[150] The Cu nanoparticles core demonstrated excellent stability that it started to be oxidized at high temperature of about 165 °C and remained unchanged upon exposure to air atmosphere for 60 d at room temperature. Furthermore, the carbon shell can efficiently protect and inhibit the oxidation or leaching of unstable NPM-based cores in harsh conditions.[100,151,152] Then, how to make the NPM-based core@carbon shell materials maintain catalytic activity is the most important point. Although the carbon shell should prevent direct contact of the metal-based core with the external environment, electrons can still be transferred from the inner NPM-based core to the ultrathin carbon shell. So as to realize the adjustment of the electronic state of the carbon shell.[153–157] The electronic interactions between the inner NPM-based core and the carbon shell as well as the induced charge redistribution activate the core–shell materials with catalytic activity. For example, when a Co core is confined in the carbon shell, theoretical studies pointed to about 0.7 electrons which are transferred from the Co core to the nearby carbon shell, resulting in decreasing the local work function and adjusting the electronic density of states (DOS) of the carbon shell, which further led to significantly enhanced electrocatalytic activity.[158] Moreover, introducing heteroatom doping into the carbon shell and regulating the thickness of carbon shell are two effective ways to improve the catalytic performance of NPM-based core@carbon shell electrocatalysts via electron interaction. Hence, the relationship between the fundamental confinement effect and the enhanced performance of NPM-based core@carbon shell electrocatalysts should be elaborated. In this section, the component of carbon shell will be the main focus of attention. Unary NPM@carbon shell electrocatalysts were taken as examples to fully illustrate the confinement effect and corresponding synergy effects for better understanding the advantages and features of these confined electrocatalysts with superior activity and stability compared to NPM-based electrocatalysts without carbon shell confinement.

A typical confinement structure is composed of a unary NPM core and a pure carbon shell (**Figure 4**A). Sharma et al. reported one or two graphene layer-encapsulated Co nanoparticles adhered to carbon black (Co@G/C).[83] Due to the confining graphene shell, the Co nanoparticles had an average diameter of 4.1 nm and were well isolated from other nanoparticles to prevent the Co nanoparticles from sintering during the pyrolysis. The X-ray absorption near-edge structure (XANES) and extended X-ray absorption fine structure (EXAFS) spectra clearly indicated that Co@G/C had only metallic Co nanoparticles without Co oxides (Figure 4B). Due to the nanostructure, Co@G/C had a comparable half-wave potential (HP) at 0.80 V (Note: all potentials in this review are versus a reversible hydrogen electrode, unless otherwise specified.) to that of commercial Pt/C catalyst in 0.1 M KOH. Co@G/C also showed a higher durability than the commercial Pt/C catalyst after 5000 cycles of the accelerated durability test. The shell prevented the Co core from corroding and migrating in strong alkaline solution, while commercial Pt/C catalyst showed an obvious agglomeration after the accelerated durability test. Subsequently, theoretical calculations were used to study the mechanisms of the Co@G/C for ORR. Previous study had already shown that the interaction between the inner NPM core and the carbon shell could not only modify the DOS around the Fermi level, but also promote the charge transfer from the NPM core to the carbon shell.[160] Therefore, the work function value of Co@graphene shell (Co@G) is 3.18 eV, which is lower than that of freestanding graphene (4.46 eV) (Figure 4C). A reduced work function of Co@G makes it easier to donate electrons from its surface to the adsorbed O_2 because of a lower energetic barrier. Compared to freestanding graphene, Co@G had a stronger interaction between the carbon shell surface and the O_2, resulting in better ORR performance. The theoretical calculations portended that the carbon shell with reduced work function may be the active site. Whereas, experimental verification was also necessary. Since CN^- anions strongly interact with metal surfaces rather than the carbon surfaces (including N-doped or pristine carbon structures) in alkaline solution, the CN^- poisoning test was used to further evaluate whether Co core or carbon shell acts as the catalyst. The almost fully recovered ORR activity of Co@G/C seemed to prove that the carbon shells are the main active sites in the electrocatalytic reaction. In contrast, commercial Pt/C lost its activity after CN^- poisoning and hardly recovered after cleaning by water. Meanwhile, a CO stripping test indicated that a small number of the Co atoms in the Co core were exposed on the carbon shell, due to the voids in the carbon-ring structure of the carbon shell. The slight decrease of the recovered activity of Co@G/C was attributed to the formation of $K^+(H_2O)_x$–CN clusters on the exposed Co sites, which blocked the nearby active carbon sites. It seems that both the Co core and the carbon shell worked as the catalytic sites. Furthermore, Co atoms with different exposure ratios in Co@G/C were obtained by adjusting the pyrolysis temperature. The higher the pyrolysis temperature, the smaller the number of the exposed Co atoms, because the carbon shell became denser and higher crystallinity. Interestingly, the ORR activities of the Co@G/C with different exposed Co atoms were almost the same before CN^- poisoning. In consequence, these results confirmed that the carbon shell covering the Co core worked as the main and only active site.

However, Ai et al. presented a different viewpoint, namely that the NPM core may act as the main active sites, by studying a Ni@carbon shell electrocatalyst.[64] The pure carbon shell without the Ni core showed an overpotential of 900 mV (Note: all overpotentials in this review are obtained at a current density of 10 mA cm^{-2}, unless otherwise specified.), which was a very poor HER activity. After introducing the Ni core, the overpotential decreased to 240 mV. Further SCN^- poisoning tests showed an obvious increase of the overpotential by around 150 mV after the electrocatalyst was treated by SCN^-, which was also better than the pure carbon shell. The reason for this result is that SCN^- poisoned some metal sites. Meanwhile, with the pyrolysis temperature increasing from 600 °C to 800 °C, the catalytic activity obviously decreased. Hence, the researchers suggested that the

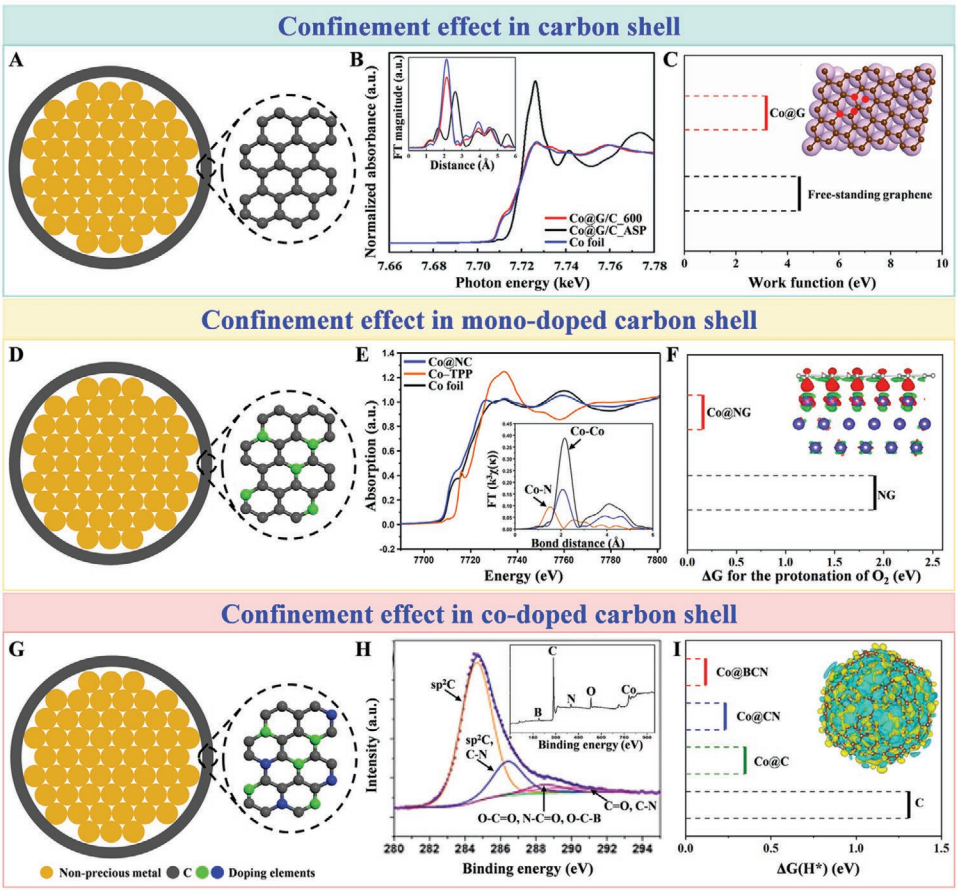

Figure 4. A) Schematic illustration of unary NPM confined in pure carbon shell. B) XANES spectra of Co@G/C_600 (G is graphene, C is carbon block and 600 is calcination temperature), Co@G/C_ASP (ASP is as-prepared precursor), and Co foil. Inset is the EXAFS spectra. C) The work function of Co@G and free-standing graphene. Inset is the top view of the Co@G system. Purple and small brown spheres represent Co and C, respectively. Red dots indicate probable adsorption sites of O at the Co@G system. D) Schematic illustration of unary NPM confined in monoelement-doped carbon shell. E) XANES spectra of Co@NC, commercial cobalt(II) tetraphenylporphyrin (Co-TPP) and Co foil. Inset is the EXAFS spectra. F) Free energy (ΔG) for the protonation of O_2 of Co@NG and NG (NG: N-doped graphene). Inset is the side view of the difference charge density plot of NG supported on a Co substrate. The gray, dark blue, and light blue balls represent C, N, and Co atoms, respectively. G) Schematic illustration of unary NPM confined in two-element-doped carbon shell. H) C 1s XPS spectra of Co@BCN. Inset is the full XPS spectrum of Co@BCN. I) the free energy for H adsorption (ΔG(H*)) of the HER on Co@BCN, Co@CN, Co@C, and C, respectively. Inset is the 3D charge density difference for Co@BCN. Yellow and blue isosurfaces represent charge accumulation and depletion, respectively. B,C) Reproduced with permission.[83] Copyright 2019, Royal Society of Chemistry. E,F) Reproduced with permission.[87] Copyright 2017, American Chemical Society. H,I) Reproduced with permission.[79] Copyright 2015, American Chemical Society.

Ni cores acted as the active sites. Nevertheless, if the Ni core was the only catalytic site, the catalytic activity of the Ni@carbon shell after SCN^- poisoning (≈390 mV) should be almost the same as the pure carbon shell without the Ni core (≈900 mV). But the result was not the case. Judging from a large number of related published papers, introducing Ni core indeed activated the carbon shell, so both the Ni core and the carbon shell may act as the catalytic sites. Moreover, Yang et al. also thought the carbon shell was the minor active phase while the NPM-based core is the main active component by comparing the catalytic activity of the pure carbon shell and the NPM-based core@carbon shell.[124] Therefore, the catalytic active sites were both the core and the shell. Taking into account the differences of different catalysts and catalytic reactions, the evaluation of catalytic active sites in NPM-based core@carbon shell electrocatalysts is worthy of in-depth study in the future.

To further tune the electronic properties and catalytic performance in core–shell electrocatalysts, heteroatom doping with nonmetallic elements in the carbon shell has been proven to be an effective strategy (Figure 4D). On the basis of molecular orbital theory, different electronegativities of diverse doping atoms would tailor the electronic structure of nearby C atoms at different levels, which lead to different adsorption energies of intermediates.[89] Furthermore, doping in general can even turn inert or inferior materials into active catalysts by activating more efficient active sites near the doping atoms to endow the materials with more novel catalytic functions.[159] Nitrogen, as an n-type carbon dopant, could further modulate the electron distribution relative to the pure carbon shell. Nitrogen is also the most commonly used dopant to form disordered carbon nanostructures, create more active sites for electrocatalysis and promote the transfer of electrons to the nearby C atoms.[160–162]

For example, Zhang et al. successfully synthesized Co nanoparticles encased in an N-doped carbon shell (Co@NC) via a N-heterocyclic carbene (NHC)–Co precursor without Co–N coordination, which ensured that nitrogen only doped into carbon shell (Figure 4E).[87] Taking the Co (111) surface covered by a layer of N-doped graphene (Co@NG) as a simplified model, the calculated DOS at the Fermi level of N-doped graphene was increased after doping N atoms into the pristine graphene. Meanwhile, the calculated DOS reflected a strong coupling between the d orbitals of the Co atoms and the p orbitals of the C and N atoms in Co@NG. Bader charge analysis indicated that about 3 electrons are transferred from Co to the N-doped carbon shell, which also enhanced the Fermi energy level of N-doped graphene. The charge on NG is redistributed after encapsulating Co (inset in Figure 4F). Hence, the shift of the work function and the charge transfer were beneficial to improving the electrocatalytic performance. N-doping into the carbon layer can reduce the dissociative adsorption energies of O_2 on the carbon layer compared to the undoped one, which had a positive effect for ORR.[161] To further understand the possible effects of the Co substrate under N-doped graphene on the four-electron ORR process, the free energy was calculated in every elementary step of the ORR reaction. Moreover, the ΔG evaluated by density functional theory (DFT) calculations for the protonation of O_2 (the rate-determining step in the ORR process) with Co@NG was 0.154 eV, much lower than that of pristine NG (1.91 eV), manifesting that Co core confined in N-doped carbon shell could lead to a better ORR activity (Figure 4F). In 0.1 M KOH, Co@NC had a somewhat more positive HP of ≈0.85 V than that of the commercial Pt/C (0.84 V). Furthermore, Co@NC retained about 95% of the initial current density after 20 000 s at 0.75 V, whereas the commercial Pt/C only maintained about 60%. Therefore, both DFT calculations and experimental results suggested that Co@NC should have enhanced ORR activity and stability. However, there is a universal problem that N doping usually results in several coexisting N-atom types, including graphitic N, pyridinic N, pyrrolic N, and quaternary N. Different types of N in the carbon shell may play a different role in adjusting the electrocatalytic performance. There is a lack to precisely control the types and percentage of N doping.[89,107] In addition, the work function is not the only factor that can impact on the ORR, the percentage of effective adsorbing oxygen sites need to be considered. Although Co@G and N-doped graphene have almost the same calculated work function, Co@G had much more active sites (86%) for adsorbing oxygen than N-doped graphene (7%) which led to a better ORR performance.[83]

Furthermore, two nonmetallic element-doping with opposite electronegativity to that of carbon, could activate adjacent C atoms by a coupling effect and, thereby, enhance catalytic activity (Figure 4G).[163,164] For example, Zhang et al. prepared a B,N-codoped ultrathin carbon shell encapsulated Co nanoparticles (Co@BCN) (Figure 4H).[79] Co@BCN showed the lowest overpotential in HER compared to Co@CN, Co@C, and commercial Co/C in both acidic and alkaline solution. Moreover, Co@BCN had a stable electrocatalytic activity after 2000 cyclic voltammetry (CV) cycles and generally maintained its initial current density over 10 h. Combining with DFT calculations, the free energy for H adsorption (ΔG(H*)) on the pure carbon shell was 1.31 eV, which was too weak. The adsorption of the H atom on pure carbon shell was thermodynamically unstable. When introducing the Co core into the carbon shell, the charge transfer from the core to the carbon shell modified the electronic structure near the Fermi level of carbon shell. The enriched charge density of carbon shell would effectively stabilize the H* species. Therefore, ΔG(H*) of Co@C obviously decreased to 0.35 eV and the activity of HER is significantly improved. As the doping elements increase from one (N) to two (B and N), the coexistence of B and N atoms in the carbon shell could coactivate the adjacent C atom in the carbon shell by affecting its valence orbital energy levels and leading to a further reduced H atom adsorption (ΔG(H*)) (0.118 eV, * denotes a free active site on the electrocatalyst model), which was closer to 0 eV than other model catalysts, implying a more suitable H atom adsorption–desorption property of the codoped carbon shell (Figure 4I).[165,166] Hence, the Co@BCN had the best HER performance. Besides the Co and Ni cores mentioned above, other unary NPMs (e.g., Fe@carbon shell loading on single-walled carbon nanotube (SWCNT), Cu@N-doped carbon shell) could also be used in core–shell structural electrocatalysts.[60,78]

In addition, some reports indicate that the electron penetration from the metal core to the outer part of the surrounding carbon shell can be affected by the thickness of the carbon shell.[160,161] From the theoretical calculation, it can be seen that the NPM cores could hardly affect the outermost carbon layer with an overthick carbon shell. Although electrons can penetrate three-carbon shells, the effect of the core on the carbon shell would notably decline with an increase in the number of carbon shell layers from one to three.[93,160] Hu et al. constructed 1–2, 2–3, and 3–5 layers of carbon shell structure on the same NPM core by adjusting the time of CVD. The electrocatalytic tests indicated that the activity decreases with the increase of the shell thickness.[93] Both of the theoretical calculation results and the experiment results showed that the carbon layer thickness has a substantial influence on the catalytic activity, and the thinner the carbon shell, the higher the catalytic activity, irrespective of whether an alloy or single metal core is confined within the carbon shell.[91,93,145] In recent years, Bao and co-workers have realized a controllable synthesis of a series of NPM cores individually confined in single layer or double layer of carbon shells, thereby effectively enhancing the catalytic activity.[91,110,111] While paying attention to the significant increase in activity by reducing the layer number of the carbon shell, it is also necessary to note that the ultrathin carbon shell will cause the severe dissolution of the NPM core, thereby reducing catalytic durability in harsh environments.[93] And the carbon shell could also be dissolved during the electrocatalytic process.[128] Meanwhile, some carbon shells with a thickness of more than three layers also showed a good electrocatalytic performance.[60,84,102] Therefore, a balance between electrocatalytic activity and chemical stability still needs further in-depth study.

In general, diverse NPM-based cores encased in various carbon shells structures induce different changes of work function and electron states. This can thus promote the NPM-based core@carbon shell electrocatalysts for various electrocatalysis, including HER, ORR, and OER.[80,82,86] Although the confinement structure endows the electrocatalysts with good catalytic performance, the challenges of clearly verifying the real active

centers in the core–shell electrocatalysts and evaluating the effective active sites on carbon shell with or without heteroatom doping remain to be completely resolved in the future.

4. Confinement Effects of NPM-Based Cores

For carbon-shell-encapsulated unary-NPM electrocatalysts, the confinement effect provides an apparently effective way to not only protect the metal core but also enhance the electrocatalytic performance. With more in-depth research and exploration of optimizing the core–shell nanostructure and electrocatalytic performance, designing novel NPM-based core@carbon shell materials is widely adopted.[85,122,167] Recently, alloying, doping, and heterojunction constructing are the three main strategies for modulating the NPM-based cores in order to design appropriate core–shell catalysts in different electrocatalytic systems (**Figure 5**).[67,111,168] In this review, alloying design particularly means the combination of no less than two kinds of different elements (including at least one metallic element) of similar amounts, so that the final core has the new alloy properties compared to the single element core. Whereas the doping design mainly refers to the introduction of small amount of heteroatom elements (including metallic elements and nonmetallic elements) into the NPM-based cores. After doping, the crystal structure of the parent cores has not changed. This section elaborates on these three effects (alloying, doping, and heterojunction) in confinement structures and how they modulate the electrocatalytic performance by altering the electronic structure in the core–shell electrocatalysts shown by theoretical or experimental results. It is emphasized that all three effects impact on the performance of the core–shell electrocatalysts with its confinement structure.[71,74]

4.1. Alloying Effect

Alloys have been widely used in catalysis for several decades. The alloying at the nanoscale endows an effective way to tune the chemical, electronic, and even magnetic interactions between different metal components and combining different properties of each pure metal component.[169–171] Numerous reports indicate that the alloyed catalysts can show a higher activity or selectivity to a certain degree, over the individual components.[89,106] Strain effect, ligand effect, and ensemble effect in the alloying metals would affect their physicochemical property in terms of geometry, electronic property, and coordination situation, thereby modulating their catalytic performance. In reality, two or even three of these changes will exist simultaneously.[70,172,173] Furthermore, alloying another element

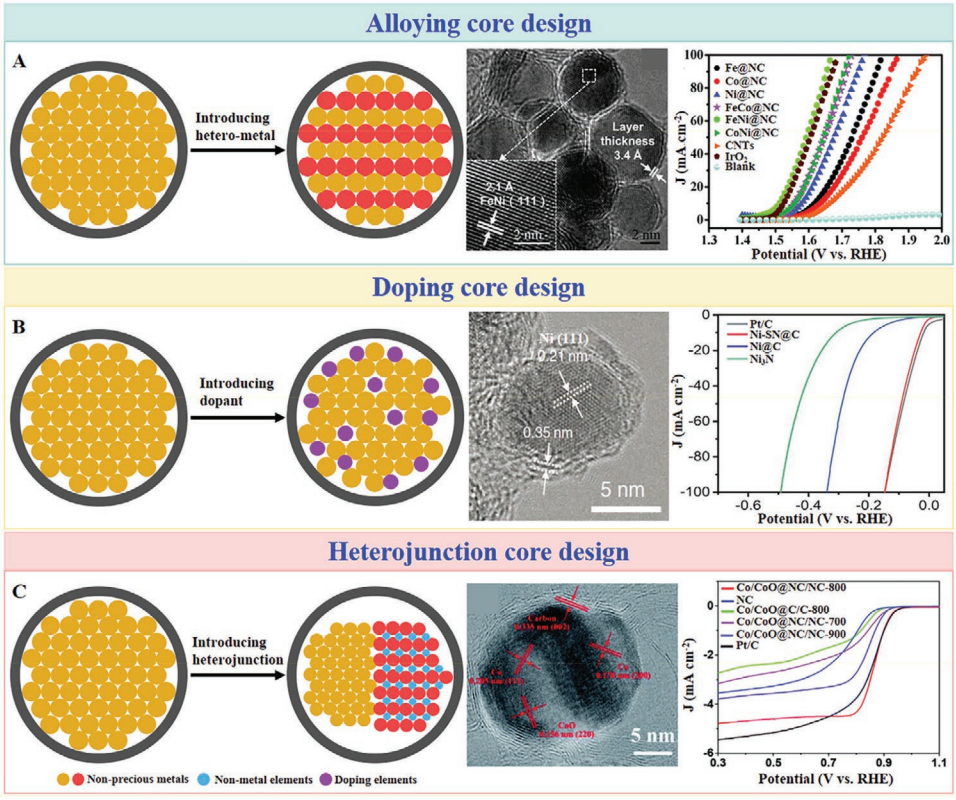

Figure 5. Schematic illustration of modulating NPM-based cores: A) alloying, and a typical example of NPM alloying core@carbon shell electrocatalysts for OER, B) doping, and a typical example of surface N-doped Ni core@carbon shell electrocatalysts (Ni-SN@C) for HER, C) heterojunction, and a typical example of Co/CoO heterojunction core@carbon shell electrocatalysts for ORR. TEM image and linear sweep voltammetry (LSV) curves in A) Reproduced with permission.[111] Copyright 2016, Royal Society of Chemistry. TEM image and LSV curves in B) Reproduced with permission.[67] Copyright 2021, Wiley-VCH. TEM image and LSV curves in C) Reproduced with permission.[168] Copyright 2018, Royal Society of Chemistry.

into a pristine single metal can inhibit side reactions or promote antipoisoning ability in a catalytic process to some extent.[147,174] However, bare NPM alloy electrocatalysts still have an unsatisfactory activity and poor stability in harsh environments. To address these issues, NPM alloy cores were confined in conductive carbon shells.[57,72] Due to the difference in atomic radius, the bond length between the heteroatoms in the alloy core has changed compared to the unary core, and the d-band center has also shift. The change in the overall electronic state of the alloy core certainly would influence the electronic situation of the closely connected carbon shell. Compared with unary NPM core@carbon shell electrocatalysts, the ability of the catalysts to adsorb or desorb intermediates can be further optimized by introducing suitable alloying elements into the unary NPM core.[89,106,111] Hence, the alloying effect in confinement structure should enhance the performances of both catalytic activity and stability. Numerous experimental and theoretical studies were conducted in the hope of in-depth understanding the main reason for improved performances.[111,128]

Multimetallic alloying is an important part of alloy core design (**Figure 6**A). For example, Bao and co-workers conducted a series of research on binary alloy cores confined in carbon shells as catalysts in electrocatalysis. They successfully prepared a series of ultrathin graphene shell confining NPM cores via CVD or pyrolysis.[110,111,143] The representative product consisted of FeNi alloy nanoparticles with the average size of 4–6 nm and a 1–4 layer graphene shell (FeNi@G, Figure 6B).[110] The optimal overpotentials of Fe_xNi_{1-x}@G ($x = 0$, 0.25, 0.5, 0.75) occurred when the content of Fe was 50%, thus FeNi@G displayed the smallest overpotential of 280 mV in comparison with any other samples and even commercial IrO_2 for OER in 1.0 M KOH solution. The experimental overpotentials increased in the following order: FeNi@G < $FeNi_3$@G < Fe_3Ni@G < Ni@G (Figure 6C). The potential of FeNi@G was kept stable at a current density of 10 mA cm^{-2} for 24 h. Due to the different atomic radius and electronegativity of Fe and Ni, the formation of bonds and change of the bond length led to the ligand effect and strain effect which finally brought about a shift of d-band center in binary core and an optimized free energy with the reactants and intermediates.[175,176] From the DFT calculations, the free energies of HOO* (ΔG(HOO*)) and HO* (ΔG(HO*)) on different surfaces had a universal scaling relation, in which the different values between ΔG(HOO*) and ΔG(HO*) for different models were all ≈3.2 eV.[111,177] Hence, the theoretical overpotential was determined by ΔG(HO*) and ΔG(O*). Using this theoretical model, it is possible to predict the overpotential of NPM-based core@carbon shell electrocatalysts in OER. By calculating the free energies of various intermediates for the OER over Fe_xNi_{1-x}@G, the electronic properties of the graphene shell could be significantly adjusted by electrons transfer after introducing Fe_xNi_{1-x} core and N-doping in the graphene shell, which further change the binding energies of intermediates on the graphene shell surface. Moreover, it showed that the too strong binding of O* on Fe@G would block the active sites, which led to a much higher overpotential. When using Ni to replace Fe in the core, the free energy of all intermediates increased. Meanwhile, the number of charge transfer from the alloying core to the graphene shell layer was increased with the Fe content decrease. This result indicates that Fe core may have a more significant activation effect on graphene shell compared to Ni core. Hence, the ΔG(HO*) decreased with the increase of Fe (inset in Figure 6C), indicating a weak

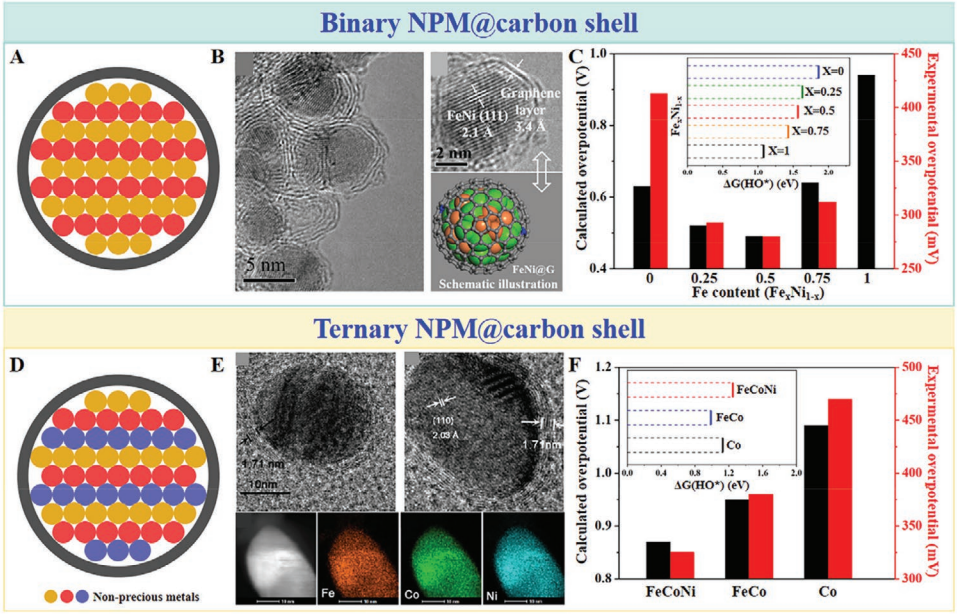

Figure 6. A) Schematic illustration of binary NPM@carbon shell. B) High resolution TEM images and schematic illustration of FeNi@G. C) The calculated and experimental overpotential of Fe_xNi_{1-x}@G for OER. Inset is the free energies of HO* (ΔG(HO*)) of Fe_xNi_{1-x}@G. Here *X* was 0, 0.25, 0.5, 0.75, 1, respectively. D) Schematic illustration of ternary NPM@carbon shell. E) High-resolution TEM images, scanning TEM image and elemental mapping images of FeCoNi@G. F) The calculated and experimental overpotential of Co, FeCo, and FeCoNi cores confined in graphene layers for OER. Inset is the free energies of Co, FeCo, and FeCoNi cores confined in graphene layers. B,C) Reproduced with permission.[110] Copyright 2018, Elsevier Ltd. E,F) Reproduced with permission.[101] Copyright 2016, American Chemical Society.

adsorption of HO*. However, the calculated overpotential showed a reversed volcano curve with Fe content increasing. As the content of Fe increased from 0% to 50%, the calculated overpotential decreased, and increased again when the content of Fe increased from 50% to 100%, which were consistent with the experimental results (Figure 6C). The trends between the calculated overpotential and ΔG(HO*) with the increase of Fe content in Fe_xNi_{1-x}@G were different because the adsorption strength of the intermediates and the balance of each intermediate synergistically influenced the overpotential during multiple elementary steps of the OER process. When the Fe/Ni ratio was about 1, the theoretical and experimental results show the optimal activity at the same time.

Moreover, three different kinds of NPM elements were used to compose an alloy core (Figure 6D). For example, Yang et al. prepared different ratios of ternary FeCoNi alloys confined in graphene layers (FeCoNi@G, Figure 6E).[101] Among all samples, FeCoNi@G with the mole ratios close to 3:4:3 had the lowest overpotential of 325 mV, which was superior to FeCo@G, FeNi@G, CoNi@G, and Co@G. It also had the best stability in an alkaline electrolyte for 10 000 cycles with negligible activity change. Although the ΔG(HO*) of the binary FeCo alloy core confined in carbon shell had the smallest value, the calculated overpotential showed an increased trend from ternary FeCoNi to unary Co core, which was consistent with the experiment results. (Figure 6F). When the Fe/Co/Ni ratios changed to 4:4:2 and 2:4:4, the experimental overpotentials increased in the following order: 3:4:3 < 2:4:4 < 4:4:2. However, it should be noted that in the theoretical calculation of HER, FeCo@G has the best ΔG(H*), which is consistent with the experimental results that FeCo@G had the smallest overpotential even than FeCoNi@G. To further reveal the different activity between in HER and OER here, charge analysis was employed. Introducing other metal atoms to form alloy would cause the strain or ligand effects, which modified the surface electron distribution of an alloy. Therefore, the number of electrons transferred from different alloy cores to the shell is different, which led to different binding energies of intermediates. As for HER, FeCo alloying core with the most transferred electrons to the graphene shell exhibited the best HER performance. With respect to OER, the overpotential was related to the ΔG(O*) and ΔG(HO*). A proper number of transferred electrons were needed, not as many as possible. This reason resulted in a volcano plot of the OER activity. Consequently, there were no clear advantages of combining metal elements in a ternary alloy core for all electrocatalytic reactions. Due to many influencing factors in an electrocatalytic process for a ternary alloy core confined in a carbon shell, the performance was not necessarily better than that of binary alloys in electrocatalytic systems.[128] Further understanding is needed to adapt the multi-metallic alloy core to the overall design of electrocatalysts and the target electrocatalytic reaction in order to achieve an improvement.

Nonmetal elements are also an alternative choice for designing alloy cores. When the alloying nonmetallic element amount reaches the same order of magnitude as the NPM atoms, the lattice constant will change from pure unary metal to metallic compound (denoted as unary NPM compound core, **Figure 7**A), which display interstitial alloying metal properties.[178,179] For example, Liu et al. reported a core–shell electrocatalyst composed of ultrasmall Mo_2C nanoparticles confined in N-doped carbon nanolayers (Mo_2C@NC) (Figure 7B).[96] Due to the protection by the carbon shell, Mo_2C@NC showed an overpotential of 124 mV in 0.5 M H_2SO_4. Meanwhile, it also exhibited an excellent stability for 80 h at –0.07 V. Theoretical calculations indicated that N doping of the carbon shell facilitated the transfer of electrons from adjacent C to N atoms in Mo_2C@NC (inset of Figure 7B). It clearly showed a $Mo_2C \rightarrow C \rightarrow N$ electron-transfer process in Mo_2C@NC, with the adjacent C atoms to N atoms as electron acceptors from Mo_2C and electron donors to N. This result indicated that Mo_2C and N doping atoms had a synergistic effect, which made the C atoms adjacent to N atoms in the carbon shell with unprecedented catalytic activity. The absolute value of the calculated ΔG(H*) for Mo_2C@NC was the closer to 0 than for Mo_2C@C, Mo_2C, NC, and C alone (Figure 7C). This result suggested Mo_2C@NC as a highly efficient catalyst in HER.

Furthermore, a core composed of two metallic elements alloyed with one nonmetallic element (Figure 7D), namely binary NPM compound, confined in a carbon shell exhibited a better electrocatalytic performance over the unary NPM compound@carbon shell and the binary NPM compound without carbon shell.[68,109] For instance, Gu et al. successfully synthesized a bifunctional HER and OER electrocatalyst which consisted of $FeNi_3N$ nanoparticles confined in a graphitic carbon shell supported on reduced GO (labeled as $FeNi_3N$@C/RGO, Figure 7E).[102] Theoretical calculations showed that the d orbitals of Ni and Fe, and the p orbitals of N contribute to the total DOS of $FeNi_3N$ (111). It suggests more electrons (1.78 e^-) being transferred from $FeNi_3N$ to RGO than from the single-metal nitrides Ni_3N (1.16 e^-) and Fe_2N (0.81 e^-), leading to charge redistribution at the interface of $FeNi_3N$ (111)/RGO (inset in Figure 7E). The abundant electron accumulation on RGO in $FeNi_3N$ (111)/RGO enhanced the adsorption capacity of the intermediate being close to Pt and improved the HER activity (Figure 7F). The experimental overpotential of $FeNi_3N$@C/RGO was 94 mV in 1.0 M KOH for HER, which was superior to Ni_3N@C/RGO (156 mV), Fe_2N@C/RGO (195 mV), and $FeNi_3N$ (235 mV). Meanwhile, the activity of $FeNi_3N$@C/RGO remained nearly constant after the stability test. The OER experimental results had almost the same trend as HER in 1.0 M KOH. All these results indicated that $FeNi_3N$@C/RGO exhibited good activity and stability as a bifunctional electrocatalyst. In addition, Li et al. found that the electrocatalytic performance could be enhanced when the individual NPM compound@carbon shell achieved long-range order.[68] An ordered CoMnO@N-doped carbon shell superlattice structure showed a better HER and OER performance than the disordered CoMnO@N-doped carbon shell nanoparticles and even an ordered CoMnO@carbon shell superlattice structure without N-doping in the carbon shell. Hence, these NPM compounds as core with a carbon shell, can exhibit higher activity and stability for different electrochemical reactions. Often an alloy core confined in a carbon shell is reported with a better catalytic activity and stability.[103–105] But this does not mean that every alloy or an alloy per se will perform better, as alloys with worse performance over the unary core may simply not be published.

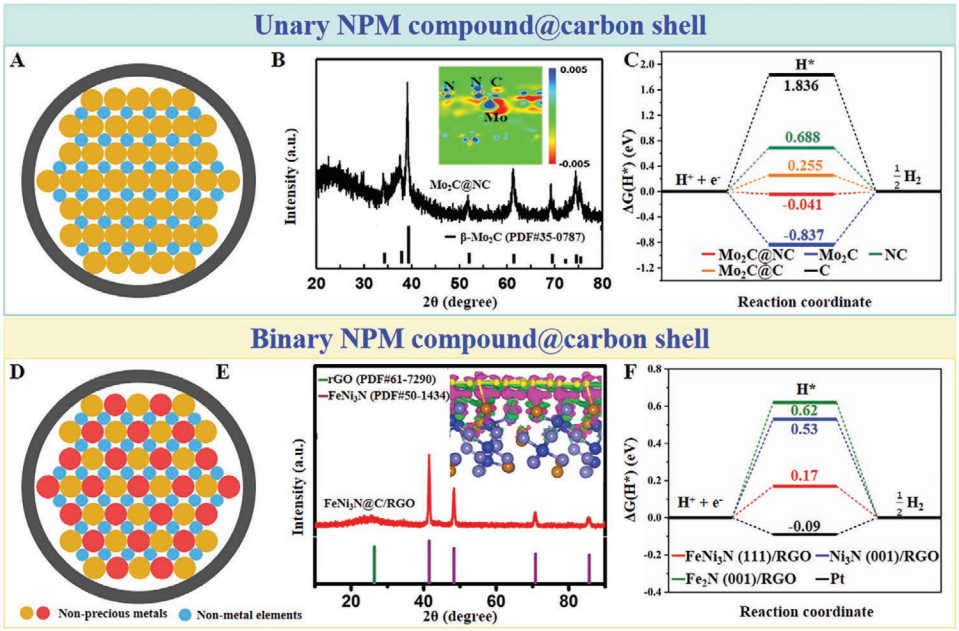

Figure 7. A) Schematic illustration of unary NPM compound@carbon shell. B) XRD pattern of Mo_2C@NC. Inset is the charge density difference from the theoretical calculation of Mo_2C@NC with the red and blue areas denoting low and high charge density, respectively (side view of the adsorption sites). C) The calculated free-energy diagram of the HER on Mo_2C@NC, Mo_2C@C, Mo_2C, NC, and C. D) Schematic illustration of binary NPM compound@carbon shell. E) XRD pattern of $FeNi_3N$@C/RGO. Inset is the charge density difference by theoretical calculation of $FeNi_3N$ (111)/RGO with the pink and green areas refer to increased and decreased charge distributions, respectively (side view of the adsorption sites). The C, N, Fe, and Ni atoms are marked in yellow, blue, brown, and wathet blue, respectively. F) The calculated free-energy diagram of the HER on $FeNi_3N$ (111)/RGO, Fe_2N (001)/RGO, Ni_3N (001)/RGO, and Pt. B,C) Reproduced with permission.[96] Copyright 2015, Wiley-VCH. E,F) Reproduced with permission.[102] Copyright 2017, American Chemical Society.

4.2. Doping Effect

For electrocatalysts confined in a carbon shell, nonmetallic elements (e.g., N, P) or metallic elements (e.g., Cr, Fe, Co, Ni) are doped into the NPM-based core by using inorganic/organic reactants, biotemplates, or MOF precursors.[112,113,117,135] Since most of the doping amount is less than 5 wt%, the parent structures are basically maintained. Nonetheless, doping in the cores, which is similar to doping heteroatoms in the carbon shell, will expectedly change the local electronic structure leading to charge redistribution at the surface and around the Fermi level, and change the coordination environment.[180–182] The goal is to balance the adsorption/desorption of reactants and intermediates, for a better catalytic performance.[183] Confined by the carbon shell, doping effect not only affect the electron structure on the surface of the NPM core, but also influence the carbon shell. This brings about changes in the binding energy to the reactants and intermediates.

Generally, the doping amount on the surface of a metal core is very small, so that it cannot affect the overall lattice parameter (**Figure 8**A). However, this doping will influence the surface electronic structure and thereby change their electrocatalytic performance. Ryu et al. developed an electrocatalyst in which Co nanoparticles with small amounts of P doped on the surface were confined in a carbon shell and anchored on carbon black (P-doped Co@C/C, Figure 8B).[117] The X-ray diffraction (XRD) peaks and transmission electron microscopy (TEM) image indicated that metallic Co was the majority in P-doped Co@C/C. Along with P-doping, the d-band center (d_{avg}) shifted from −1.93 to −1.72 eV and the oxygen binding energy on the carbon shell was enhanced (Figure 8C). The results showed that a suitable d-band center position that could well balance the adsorption of reactive intermediates and surface coverage of blocking species was needed to obtain optimal ORR kinetics. The phosphorus incorporation on the surface of the metal core endowed the catalyst with a more efficient and durable ORR activity (HP = 0.8 V) and good stability in alkaline solution. Surface nitridation on a metal core confined in a thin carbon layer also caused a charge redistribution on the catalyst surface, which exhibited a positive effect on the electrocatalytic activity and stability in electrocatalysis.[67,114]

Besides nonmetal elements, metal elements, such as Cu, Mo, could also act as dopants on the surface of the metal core to modulate the electronic structure resulting in facilitating the electrocatalytic performance.[115,118] Recently, a Mo-doped Ni core confined in an N-doped carbon shell anchored on SWCNT (Mo-doped Ni@NC/SWCNT) was reported by Majeed et al.[115] The content of Mo was only 1.8 wt% as tested by XPS. In 1.0 M KOH solution, Mo-doped Ni@NC/SWCNT had overpotentials of 130 mV and 255 mV for HER and OER, respectively. Without Mo doping, the overpotentials of Ni@NC/SWCNT would increase by 60 and 15 mV for HER and OER, respectively. In terms of stability, both the LSV curves after 5000 CV cycles and the current density after 20 h under constant potentials were nearly unchanged. Moreover, the electrocatalytic activity also became worse, as the amount of Mo increased to 2.3 and

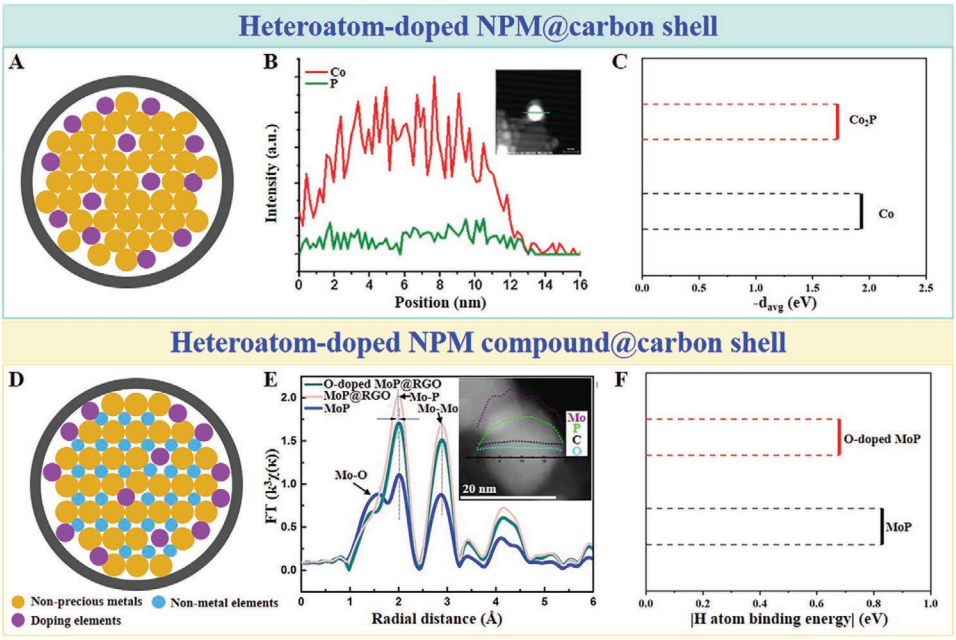

Figure 8. A) Schematic illustration of heteroatom-doped NPM@carbon shell. B) Line profile spectra of P-doped Co@C/C. Inset is the corresponding P-doped Co@C. C) d-band centers (d_{avg}) of a surface Co atom below the Fermi level on Co_2P, and Co surfaces. D) Schematic illustration of heteroatom-doped NPM compound@carbon shell. E) Fourier transform (FT) of Mo K-edge EXAFS oscillation function. Inset is the scanning TEM image of O-doped MoP@RGO and the intensities for different elements. F) The H atom binding energy bound with a P atom on a surface of O-doped MoP and neat MoP, respectively. B,C) Reproduced with permission.[117] Copyright 2014, Royal Society of Chemistry. E,F) Reproduced with permission.[62] Copyright 2016, American Chemical Society.

4.1 wt%. These results indicated that a small doping amount of Mo into the Ni core could enhance the bifunctional electrocatalytic performances. Therefore, the type and content of doping elements need to be comprehensively considered based on the parent unary NPM cores, the type of catalytic reaction, and the environment.

In addition to doping into the unary NPM cores, heteroatom doping into NPM compound cores was also reported (Figure 8D). For instance, O-doped MoP confined in RGO (O-doped MoP@RGO) was reported by Zhang et al.[62] The Fourier transform (FT) curves from Mo K-edge EXAFS oscillation function showed some peaks between 1 and 4 Å, belonging to Mo–Mo and Mo–P coordination in O-doped MoP@RGO, MoP@RGO, and MoP. It was worth noting that a new peak of O-doped MoP@RGO at around 1.5 Å was assigned to Mo–O coordination (Figure 8E). The intensities of signals for Mo, P, and a small amount of O were presented across the particle (inset in Figure 8E). The trace O doping possibly resulted in the surface structural disorder.[184] From the theoretical calculations, O-doping increased the DOS of metal atoms close to the O atom across the Fermi level, indicating enhanced conductivity of the O-doped molybdenum phosphides.[185] The incorporated O atoms led to an increase of electron concentration especially in the conduction band, facilitating charge carrier transfer during the electrocatalytic process.[186] The binding energy of an H atom on the surface is reduced after O doping into MoP (Figure 8F), which exhibited an optimal Gibbs free energy for HER. Furthermore, O-doping elongated the Mo–P bond length, weakening the H binding energy to accelerate the desorption of H_2. As a consequence, the catalytic activity eventually improved. In 0.5 M H_2SO_4 solution, the overpotential at 20 mA cm^{-2} of O-doped MoP@RGO was 118 mV, which was smaller than that of MoP@RGO (479 mV). Synchronously, introducing O-doping into CoP@RGO could also enhance the OER activity and stability.

Similarly, when NPM elements (e.g., Ni, Co, Fe, Cr) were doped into Mo_2C nanoparticles encapsulated in a carbon shell (Mo_2C@NC), the composite material showed good HER activity and stability in 0.5 M H_2SO_4.[112] The doping elements in these samples measured by energy-dispersive X-ray spectroscopy were 0.89 wt%, 3.27 wt%, 3.39 wt%, and 2.26 wt% for Ni, Co, Fe, and Cr, respectively. Both the lattice spacing in TEM images and the XRD characteristic peaks correspond to the Mo_2C structure. The trend of the overpotentials was Ni-doped Mo_2C@NC (72 mV) < Co-doped Mo_2C@NC (122 mV) < Fe-doped Mo_2C@NC (129 mV) < Cr-doped Mo_2C@NC (147 mV) < Mo_2C@NC (298 mV). The Ni-doped Mo_2C@NC also had the best stability than the other three samples after 2000 CV cycles. From the DFT calculations, $\Delta G(H^*)$ of Ni-doped Mo_2C, Co-doped Mo_2C, Fe-doped Mo_2C, and Cr-doped Mo_2C was −0.3, −0.4, −0.42, and −0.53 eV, respectively, indicating that the NPM doping could reduce the intensity of the interaction with H atoms to varying degrees compared to Mo_2C. Moreover, $\Delta G(H^*)$ obviously decreased to 0.19 eV after confining Ni-doped Mo_2C by N-doped carbon shell, leading to the best hydrogen adsorption-desorption capability. These results jointly indicated that the introduction of NPM dopants (especially Ni) into Mo_2C nanoparticles could optimize the HER activity of the catalysts. Furthermore, the doping amount of another NPM element more or less had an influence on forming partly substitutional or interstitial

doping on the NPM-based core according to the calculated formation energies, which could also have a positive or negative impact on the electrocatalytic activity.[113] Notably, doping a confinement structure in the above-mentioned electrocatalysts could improve the electrocatalytic performances, concerning both activity or stability.

4.3. Heterojunction Effect

In general, a heterojunction structure, in the presence of an electrical contact interface of two different materials, has an unequal band structure. The Fermi levels tend to balance leading to charge transfer and stretching the region of charge depletion, which is macroscopically different from their single components. The enhancement of catalytic performance of heterojunction is attributed to the electron relocalization at the interface and exposure of active sites.[123,187–189] A heterojunction structure in catalysts is widely used in numerous catalytic reactions, especially in electrocatalysis.[190–195] Constructing a carbon shell around an NPM-based nanoheterojunction to form a confinement structure could effectively provide a physical protection for the NPM-based heterojunction core, similar to the alloyed and doped structures. More importantly, the synergistic interaction, especially the electronic effect, between different components in this heterojunction core, can effectively promote the electron transfer between the two components, and it is also beneficial to promote the electron transfer from the inner NPM-based heterojunction core to the outer carbon shell, thereby improving the adsorption or activation of intermediates for boosting the electrocatalytic performance.

One kind of typical heterojunction core is composed of NPM and NPM compound (**Figure 9**A). Liu et al. developed a Ni/Ni_2P nanoheterojunction core confined in a carbon shell (Ni/Ni_2P@C) by combined carbonization and phosphorization processes.[121] The weight ratio of Ni and Ni_2P could be easily controlled by changing the amount of NaH_2PO_2 which is used as bonderite. The clear lattice fringes indicated that Ni and Ni_2P were closely connected with each other at the nanolevel, which was seen as a strong evidence of nanoheterojunctions in Ni/Ni_2P@C (Figure 9B). Compared to Ni@C and Ni_2P@C, Ni/Ni_2P@C exhibited a much better HER performance in 0.5 M H_2SO_4 with an overpotential of 149 mV and negligible negative shift of the LSV curves after 1000 cycles. The heterojunction design was deemed to play a significant role in promoting HER performance. Further DFT calculations showed that Ni/Ni_2P had a lower ΔG(H*) of –0.12 eV than those of Ni_2P (–0.23 eV) and Ni (–0.30 eV). Meanwhile, the calculated DOS manifested that the Ni/Ni_2P structure with its metallic state in contrast to single Ni and Ni_2P had an enhanced carrier density near the Fermi level (Figure 9C). These theoretical results explained the better HER electrocatalytic activity of Ni/Ni_2P, in accord with the experimental results.

Moreover, Su et al. developed a Co/Co_3ZnC nanoheterojunction core confined in a thin NG shell (Co/Co_3ZnC@NG) by thermal decomposition of Prussian blue analogs at 650 °C.[69] Above or below this temperature, Co@NG or Co_3ZnC@NG were obtained, respectively. Co and Co_3ZnC were closely connected with each other at the nanolevel, which provided strong evidence of nanoheterojunctions in Co/Co_3ZnC@NG. The XPS peaks of Zn 2p and Co 2p of Co/Co_3ZnC@NG shifted toward lower binding energies, compared to that in samples with a single component core, which suggested

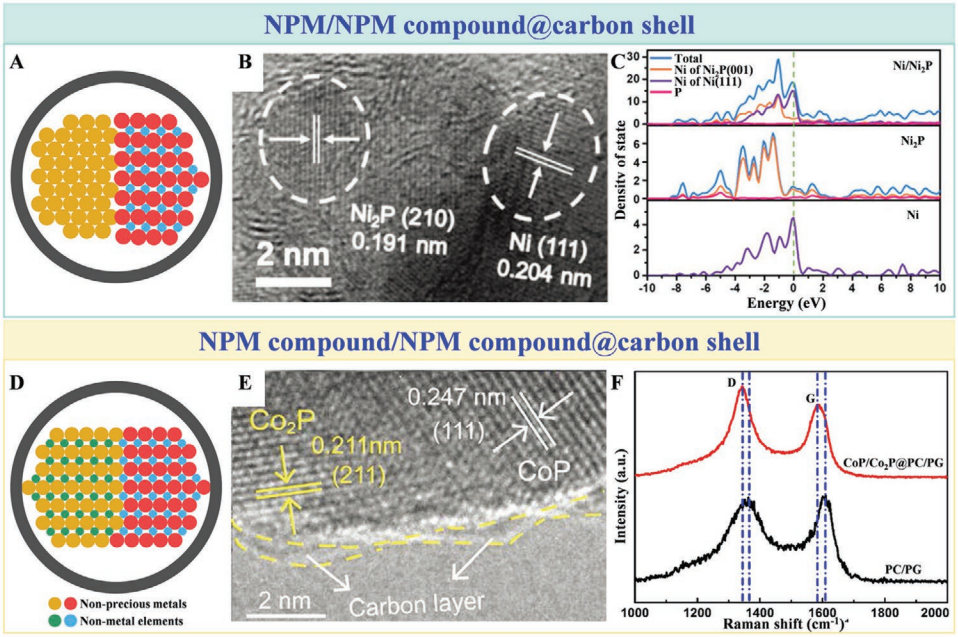

Figure 9. A) Schematic illustration of binary NPM/NPM compound@carbon shell. B) High-resolution TEM image of Ni/Ni_2P@C. C) Calculated DOS for Ni/Ni_2P, Ni_2P, and Ni. D) Schematic illustration of NPM compound 1/NPM compound 2@carbon shell. E) High-resolution TEM image for an individual CoP/Co_2P@PC core–shell nanostructure component in CoP/Co_2P@PC/PG. F) Comparison of Raman spectrum of CoP/Co_2P@PC/PG and PC/PG. B,C) Reproduced with permission.[121] Copyright 2019, Wiley-VCH. E,F) Reproduced with permission.[124] Copyright 2019, Wiley-VCH.

charge transfer from Co to Co_3ZnC. In turn, this would increase the electron–electron repulsion within the Co_3ZnC nanoparticles, implying a strong electron coupling effect. The electron state change in the heterojunction core would affect the electron redistribution on the interface between the core and the carbon shell. Besides, NG shell provided synergism with the inside Co/Co_3ZnC nanojunction and protection during electrocatalytic reaction by confinement effect. As a consequence, Co/Co_3ZnC@NG displayed the lowest overpotential of 366 mV in 1.0 M KOH for OER, superior to that of Co@NG (419 mV), Co_3ZnC@NG (380 mV), and commercial RuO_2 (377 mV).

Not only metal and metal compound but also two different metal compounds could form nanoheterojunction structures confined in carbon shell (Figure 9D). For example, Yang et al. successfully prepared a CoP/Co_2P heterojunction nanocrystals encapsulated in a P-doped carbon shell (PC) loaded on P-doped graphene (PG) nanohybrids (CoP/Co_2P@PC/PG, Figure 9E).[124] The lattice spacings and the XRD results simultaneously confirm the coexistence of the mixed-phase CoP/Co_2P component in CoP/Co_2P@PC/PG. From the Raman spectrum (Figure 9F), the peaks of CoP/Co_2P@PC/PG were redshifted about 26 cm^{-1} relative to pure PC/PG, suggesting that there existed a strong coupling effect between the CoP/Co_2P core and the PC/PG shell.[196] Therefore, the interaction between CoP/Co_2P and PC/PG affects the adsorption capacity or activation of H_2O and other intermediates during the electrocatalytic process. CoP/Co_2P@PC/PG had the best activity with an overpotential of 39 mV for HER in 1.0 M KOH, superior to other counterparts including CoP@PC/PG (46 mV), Co_2P@PC/PG (138 mV), and PC/PG (over 200 mV). The electrochemical double-layer capacitance and charge transfer resistance demonstrated that CoP/Co_2P@PC/PG had the most available active sites and the fastest interfacial electron transfer kinetics. Furthermore, CoP/Co_2P@PC/PG almost kept its initial activity after 5000 CV cycles, which showed a good stability. In the alkalic OER system, CoP/Co_2P@PC/PG still exhibited superior activity and stability over the contrast samples.

Two NPM compounds with different nonmetal elements (e.g., metal nitrides, metal phosphides) formed a nanojunction core in $Co_2P/Co_{5.47}N$ nanoparticles encapsulated in an N-doped carbon shell loaded on NG ($Co_2P/Co_{5.47}N$@NC/NG) have also been synthesized and exhibited good activity and stability for OER in 0.1 M KOH.[126] $Co_2P/Co_{5.47}N$@NC/NG needed an overpotential of 390 mV, superior to $Co_{5.47}N$/NG with an overpotential of 490 mV. It suggested that both the heterojunction core and the NC shell had positive effects for OER. However, in the above examples, an all-sided theoretical analysis of NPM-based heterojunction core@carbon shell is still lacking. Part of the research only uses experimental results and analytical characterizations to verify the performance improvement. Due to the number of the components and the diversity of the interfaces, several constructed theoretical models only considered the heterojunction core and ignored the carbon shells. This poses new challenges for the future development of mechanistic studies. Overall, these synergistic superiorities of the heterojunction in the confinement structure show a clear effect for the improvements of electrocatalytic performances.

5. Conclusions and Perspectives

Since the emergence of the NPM-based core@carbon shell structure in the 1990s, numerous research activities have continued to spring up with respect to structural design aimed at enhancing the electrocatalytic performance. In this review, an overview of recent methodologies on preparing NPM-based core@carbon shell structures was summarized. The relationship between the fundamental confinement effect and the performance improvement of the carbon shell encapsulating unary NPM electrocatalysts was subsequently elucidated. Furthermore, the effects of alloying, doping, and heterojunction in NPM-based core@carbon shell electrocatalysts in term of experimental results and theoretical calculations (when available) were fully discussed. Despite the great progress in the development of various NPM-based core@carbon shell electrocatalysts, there are still many difficulties and challenges ahead. For instance, the electrocatalysis theory relatively lags behind the development of NPM-based electrocatalysts under such rapid progress. The essence of the electronic properties on the core, core/shell interface, and shell surface are less than understood with a lack of systematic analysis. The trial-and-error methods are now conducted more commonly rather than theoretical prediction methods. To accelerate the development of NPM-based core@carbon shell electrocatalysts, the following goals are supposed to achieve in the near future.

(1) Synthesis requirement: Core@shell structure is the most common design. Many demands are required, such as the inside nanoparticles size, the outside carbon shell thickness. With reducing of the core size, subnano size might be addressed and the nanoeffect, even atom-effect, would be promoted. Note that it is not easy to tune the particle size of the NPM core in a controllable and uniform range, although the control is of vital importance in the high utilization efficiency of metal and subsequently the high transfer efficiency of electrons from core to shell. The thickness of the carbon shell is key to affect the electron penetration in different electrocatalytic reactions via experimental results or theoretical calculations. Therefore, the accurate layer number control still needs to be taken seriously, although the carbon shell can now be reduced to a single layer. Although it was reported that the thinner shell exhibited the better electrocatalytic performance, there is no clear structure–function relationship between carbon layer number and electrocatalytic stability. The compromised choice for the carbon shell was to increase the layer numbers to two to three layers. Moreover, a double-layer hybrid shell, such as layered graphene and MoS_2,[197] is also a novel idea to improve electrocatalytic performance or even realize multifunction electrocatalysis.

Furthermore, the design and synthesis of uniform size and shape within NPM-based core@carbon shell electrocatalysts are still challenging. At present, the optional shapes of the core are far from sufficient. Almost all NPM-based cores in the electrocatalysts were nanoparticles coated by a carbon shell. A few reports constructed 3D integral structures by introducing different surfactants, templates, and supports to promote matter diffusion and electron transfer, which are two important factors on influencing the electrocatalytic performance. However, the

main active components in these 3D electrocatalysts were also the nanoparticles confined in a carbon shell. It is noteworthy that designing the NPM-based core with diverse shapes (e.g., nanopolyhedron, nanowire, nanorod, nanotube, nanodendritic crystal, nanofractal structure) or high catalytic activity crystal surface is an interesting but difficult way to expose more activity sites than in simple nanoparticles.[198] These cores confined in carbon shells may change the electronic states of the carbon shell resulting in improving the active site accessibility and optimizing free energies of reactants and intermediates.

(2) Components discovery: It is well known that binary NPM alloys not only efficiently regulated the electronic structure compared to the unary NPM core, but can also integrate the advantages of the two-metal elements. Currently, a ternary NPM core confined in a carbon shell is often the limitation, but at most 15 metal elements contained in a nanoparticle have already been synthesized in the absence of the carbon shell.[199–202] Limited by the synthesis methods, it is very difficult to reach a multielement (over 3) alloyed core in a confinement structure. Therefore, the great interest arises to develop metal alloy or metal compound cores with over three metal elements. In addition, doping was another effective measure to modulate electronic properties by introducing stress, dislocation, disorder into NPM-based core or carbon shell. The controllable increase of the doping elements might be a highly encouraging approach.

Considering the heterojunctions composed of two different phases, interfacial interaction could have obviously effects on the electronic structure. The heterojunction core confined in a carbon shell could play a positive role to enhance the catalytic performance. Various methods have been used for single metal-based, alloyed metal-based or metallic compound-based core confined in carbon shell materials synthesis. It has to be pointed out that the synthesis method of NPM-based heterojunction core@carbon shell structure is still a great limitation. A single method was often only suitable for one or few specified core–shell electrocatalysts with NPM-based heterojunction core. There is still a lack of a universal way to construct numerous nanoheterojunction cores. Therefore, more routes are required for the synthesis of a rich variety of NPM compounds, not limited to pure metal, carbides, nitrides, and phosphides which are frequently used.

(3) Mechanism need: The electrocatalytic mechanism study is crucial for understanding of reaction process and enhancement of electrocatalytic performance, and also in reverse for the structural and electronic design and modulation of core–shell electrocatalysts. Although the electronic properties and catalytic nature on the NPM-based core@carbon shell electrocatalysts have been investigated by both experiments and theoretical calculations, there is a lack of effective characterization methods to in situ observe the electron transfer process and the corresponding variation of structural and electronic properties during the real electrocatalytic reaction. For example, advanced in situ scanning tunneling microscopy or TEM could provide the information on the structure, composition, and morphology of the catalysts, while in situ photoemission electron microscopy could obtain the information on the spatial distribution of adsorbates and on reaction processes.[203,204] Moreover, electronic/geometric structure, coordination environment, structural reconstruction, and catalyst-reactant/intermediate interaction could be performed by in situ X-ray absorption spectroscopy, during both the synthesis process and ongoing reaction. The in situ Raman and infrared spectroscopy could also provide the information on chemical state and phase transition, and surface adsorbates/reaction intermediates.[205,206] Hence, it is a big requirement to introduce or coalesce more effective in situ characterization techniques to understand the electrocatalytic nature and process in this NPM-based core@carbon shell electrocatalysts.

Alloying effect, doping effect, and heterojunction effect are the three most important features of NPM-based core@carbon shell electrocatalysts for enhancing electrocatalytic performance on the basis of the confinement effect. In order to study how these effects affect the electrocatalytic performance, contrast experiments are the most used methods, along with theoretical calculations at times. However, most theoretical calculations in the publications use idealized simple models. Sometimes, the detailed calculation data for core–shell electrocatalysts with almost the same composition in different studies may be a little different, although the conclusions drawn from the theoretical calculations are consistent with experimental results. Whereupon, a universal and systematic theoretical calculation system is still needed for the repeatable and in-depth analysis of the structure–effect relationship of these NPM-based cores confined in carbon shell hybrids. In addition, the definite structure provides a well-defined model to bridge the theoretic study and realistic systems, but a big gap between them still remains. This is obvious in theoretical calculations of the doped structures with multielement doping and heterojunction structures. It is also a big need to enrich and improve the theoretical calculations to study the natures of these complex structures by using more approximate models instead of simplified models or single-component models. Meanwhile, alloying effect, doping effect, and heterojunction effect have undoubtedly certain influences on electronic properties of internal NPM-based cores as well as the confinement effect. Thus, further breakthroughs in the theory of electronic energy band structure will help researchers to understand the change of the electronic structure between the core, core–shell interface, and shell more deeply and meticulously. Moreover, apart from the theoretical calculations for enhancing the activity, very little theoretical works have focused on their stability mechanism. More theoretical works should thus pay attention to the stability of structure and activity especially in long-term operation under harsh environments. With the development of the theoretical analysis basics and methods, the predictable design of electrocatalysts can be realized in the future.

Although NPM-based core@carbon shell catalysts have been studied in many fields for few decades, much remains to be learned for the fundamental research and industrial applications of these core–shell catalysts in many aspects such as electrocatalysis and industrial catalysis. The insights about structures, electronic properties, catalytic nature and process of core–shell catalysts will be increasingly enhanced. There is

a surely promising future for the advancement of this improvement by continued developments in synthetic technology, characterization science, and theoretical calculations to broaden and understand the class of these core–shell catalysts.

Acknowledgements

This work was supported by a joint National Natural Science Foundation of China-Deutsche Forschungsgemeinschaft (NSFC-DFG) project (NSFC grant 51861135313, DFG JA466/39-1), Rapid Response Bilateral Collaborative Funding of the Sino-German Centre for Research Promotion (C-0046), Fundamental Research Funds for the Central Universities (2021qntd13), Guangzhou Science and Technology Project (202102020463), Guangdong Basic and Applied Basic Research Foundation (2019A1515110436), Guangdong Province International Scientific and Technological Cooperation Projects (2020A0505100036), International Science & Technology Cooperation Program of China (2015DFE52870) and South African Research Chair (DSI/NRF/Wits SARChI Chair; UID Number: 132739).

Conflict of Interest

The authors declare no conflict of interest.

Keywords

carbon shells, confinement effects, electrocatalysis, individual encapsulation, nonprecious metal-based materials

Received: November 26, 2021
Published online: December 30, 2021

[1] S. Zaman, L. Huang, A. I. Douka, H. Yang, B. You, B. Y. Xia, *Angew. Chem., Int. Ed.* **2021**, *60*, 17832.
[2] S. Jiao, X. Fu, S. Wang, Y. Zhao, *Energy Environ. Sci.* **2021**, *14*, 1722.
[3] Z. Y. Yu, Y. Duan, X. Y. Feng, X. Yu, M. R. Gao, S. H. Yu, *Adv. Mater.* **2021**, *33*, 2007100.
[4] J. Ying, X. Y. Yang, G. Tian, C. Janiak, B. L. Su, *Nanoscale* **2014**, *6*, 13370.
[5] S. Gong, Y.-X. Zhang, Z. Niu, *ACS Catal.* **2020**, *10*, 10886.
[6] Y. Xin, S. Li, Y. Qian, W. Zhu, H. Yuan, P. Jiang, R. Guo, L. Wang, *ACS Catal.* **2020**, *10*, 11280.
[7] F. Xiao, Y. C. Wang, Z. P. Wu, G. Chen, F. Yang, S. Zhu, K. Siddharth, Z. Kong, A. Lu, J. C. Li, C. J. Zhong, Z. Y. Zhou, M. Shao, *Adv. Mater.* **2021**, 33, 2006292. .
[8] M. Li, Z. Zhao, T. Cheng, A. Fortunelli, C. Y. Chen, R. Yu, Q. Zhang, L. Gu, B. V. Merinov, Z. Lin, E. Zhu, T. Yu, Q. Jia, J. Guo, L. Zhang, W. A. GoddardIII, Y. Huang, X. Duan, *Science* **2016**, *354*, 1414.
[9] J. Ying, G. Jiang, Z. P. Cano, Z. Ma, Z. Chen, *Appl. Catal. B* **2018**, *236*, 359.
[10] Z. Ma, Z. P. Cano, A. Yu, Z. Chen, G. Jiang, X. Fu, L. Yang, T. Wu, Z. Bai, J. Lu, *Angew. Chem., Int. Ed.* **2020**, *59*, 18334.
[11] T. Wang, A. Chutia, D. J. L. Brett, P. R. Shearing, G. He, G. Chai, I. P. Parkin, *Energy Environ. Sci.* **2021**, *14*, 2639.
[12] L. Li, P. Wang, Q. Shao, X. Huang, *Adv. Mater.* **2021**, *33*, 2004243.
[13] Z. Zhang, G. Liu, X. Cui, Y. Gong, D. Yi, Q. Zhang, C. Zhu, F. Saleem, B. Chen, Z. Lai, Q. Yun, H. Cheng, Z. Huang, Y. Peng, Z. Fan, B. Li, W. Dai, W. Chen, Y. Du, L. Ma, C. J. Sun, I. Hwang, S. Chen, L. Song, F. Ding, L. Gu, Y. Zhu, H. Zhang, *Sci. Adv.* **2021**, *7*, eabd6647.
[14] J. Ying, X.-Y. Yang, Z.-Y. Hu, S.-C. Mu, C. Janiak, W. Geng, M. Pan, X. Ke, G. Van Tendeloo, B.-L. Su, *Nano Energy* **2014**, *8*, 214.
[15] L. Zhang, L. T. Roling, X. Wang, M. Vara, M. Chi, J. Liu, S. I. Choi, J. Park, J. A. Herron, Z. Xie, M. Mavrikakis, Y. Xia, *Science* **2015**, *349*, 412.
[16] J. Li, Q. Zhou, M. Yue, S. Chen, J. Deng, X. Ping, Y. Li, J. Li, Q. Liao, M. Shao, Z. Wei, *Appl. Catal., B* **2021**, *284*, 119728.
[17] Y. Nie, L. Li, Z. Wei, *Chem. Soc. Rev.* **2015**, *44*, 2168.
[18] Y. J. Wang, N. Zhao, B. Fang, H. Li, X. T. Bi, H. Wang, *Chem. Rev.* **2015**, *115*, 3433.
[19] M. Zhou, H. L. Wang, S. Guo, *Chem. Soc. Rev.* **2016**, *45*, 1273.
[20] M. F. Lagadec, A. Grimaud, *Nat. Mater.* **2020**, *19*, 1140.
[21] L. Du, V. Prabhakaran, X. Xie, S. Park, Y. Wang, Y. Shao, *Adv. Mater.* **2021**, *33*, 1908232.
[22] I. Roger, M. A. Shipman, M. D. Symes, *Nat. Rev. Chem.* **2017**, *1*, 0003.
[23] J. Zhang, J. Qian, J. Ran, P. Xi, L. Yang, D. Gao, *ACS Catal.* **2020**, *10*, 12376.
[24] L. Zhang, C. Lu, F. Ye, R. Pang, Y. Liu, Z. Wu, Z. Shao, Z. Sun, L. Hu, *Adv. Mater.* **2021**, *33*, 2007523.
[25] J. Tollefson, *Nature* **2010**, *464*, 1262.
[26] J. Masa, C. Andronescu, W. Schuhmann, *Angew. Chem., Int. Ed.* **2020**, *59*, 15298.
[27] S. L. Zhang, B. Y. Guan, X. F. Lu, S. Xi, Y. Du, X. W. D. Lou, *Adv. Mater.* **2020**, *32*, 2002235.
[28] Y. Huang, S. L. Zhang, X. F. Lu, Z. P. Wu, D. Luan, X. W. D. Lou, *Angew. Chem., Int. Ed.* **2021**, *60*, 11841.
[29] L. L. Feng, G. Yu, Y. Wu, G. D. Li, H. Li, Y. Sun, T. Asefa, W. Chen, X. Zou, *J. Am. Chem. Soc.* **2015**, *137*, 14023.
[30] J. Yang, C. Lei, H. Wang, B. Yang, Z. Li, M. Qiu, X. Zhuang, C. Yuan, L. Lei, Y. Hou, X. Feng, *Nanoscale* **2019**, *11*, 17571.
[31] L. Wu, L. Yu, F. Zhang, B. McElhenny, D. Luo, A. Karim, S. Chen, Z. Ren, *Adv. Funct. Mater.* **2020**, *31*, 2006484.
[32] L. Zhang, Y. Zheng, J. Wang, Y. Geng, B. Zhang, J. He, J. Xue, T. Frauenheim, M. Li, *Small* **2021**, *17*, 2006730.
[33] G. Yang, J. Zhu, P. Yuan, Y. Hu, G. Qu, B. A. Lu, X. Xue, H. Yin, W. Cheng, J. Cheng, W. Xu, J. Li, J. Hu, S. Mu, J. N. Zhang, *Nat. Commun.* **2021**, *12*, 1734.
[34] M. Tong, F. Sun, Y. Xie, Y. Wang, Y. Yang, C. Tian, L. Wang, H. Fu, *Angew. Chem., Int. Ed.* **2021**, *60*, 14005.
[35] X. Y. Yang, L. H. Chen, Y. Li, J. C. Rooke, C. Sanchez, B. L. Su, *Chem. Soc. Rev.* **2017**, *46*, 481.
[36] H. Wei, Z. Y. Hu, Y. X. Xiao, G. Tian, J. Ying, G. Van Tendeloo, C. Janiak, X. Y. Yang, B. L. Su, *Chem. Asian J.* **2018**, *13*, 1119.
[37] W. Liu, D. Zheng, T. Deng, Q. Chen, C. Zhu, C. Pei, H. Li, F. Wu, W. Shi, S. W. Yang, Y. Zhu, X. Cao, *Angew. Chem., Int. Ed.* **2021**, *60*, 10614.
[38] Z. Liang, N. Kong, C. Yang, W. Zhang, H. Zheng, H. Lin, R. Cao, *Angew. Chem., Int. Ed.* **2021**, *60*, 12759.
[39] Y. X. Xiao, J. Ying, G. Tian, X. Q. Zhang, C. Janiak, K. I. Ozoemena, X. Y. Yang, *Chem. Commun.* **2021**, *57*, 986.
[40] J. Zhu, L. Xu, Z. Lyu, M. Xie, R. Chen, W. Jin, M. Mavrikakis, Y. Xia, *Angew. Chem., Int. Ed.* **2021**, *60*, 10384.
[41] D. H. Kweon, M. S. Okyay, S. J. Kim, J. P. Jeon, H. J. Noh, N. Park, J. Mahmood, J. B. Baek, *Nat. Commun.* **2020**, *11*, 1278.
[42] J. Balamurugan, T. T. Nguyen, N. H. Kim, D. H. Kim, J. H. Lee, *Nano Energy* **2021**, *85*, 105987.
[43] L. Shen, J. Ying, G. Tian, M. Jia, X. Y. Yang, *Chem. Asian J.* **2021**, *16*, 1130.
[44] J. Ying, Z. Y. Hu, X. Y. Yang, H. Wei, Y. X. Xiao, C. Janiak, S. C. Mu, G. Tian, M. Pan, G. Van Tendeloo, B. L. Su, *Chem. Commun.* **2016**, *52*, 8219.
[45] Y. L. Wu, X. Li, Y. S. Wei, Z. Fu, W. Wei, X. T. Wu, Q. L. Zhu, Q. Xu, *Adv. Mater.* **2021**, *33*, 2006965.
[46] L. J. Hillenbrand, J. W. Lacksonen, *J. Electrochem. Soc.* **1965**, *112*, 245.
[47] G. Che, B. B. Lakshmi, E. R. Fisher, C. R. Martin, *Nature* **1998**, *393*, 346.

[48] G. Che, B. B. Lakshmi, C. R. Martin, E. R. Fisher, *Langmuir* **1999**, *15*, 750.
[49] S. H. Joo, S. J. Choi, I. Oh, J. Kwak, Z. Liu, O. Terasaki, R. Ryoo, *Nature* **2001**, *412*, 169.
[50] E. S. Steigerwalt, G. A. Deluga, C. M. Lukehart, *J. Phys. Chem. B* **2002**, *106*, 760.
[51] Y. Si, E. T. Samulski, *Chem. Mater.* **2008**, *20*, 6792.
[52] Y.-X. Xiao, J. Ying, G. Tian, Y. Tao, H. Wei, S.-Y. Fan, Z.-H. Sun, W.-J. Zou, J. Hu, G.-G. Chang, W. Li, X.-Y. Yang, C. Janiak, *Appl. Catal., B* **2019**, *259*, 118080.
[53] F. Afsahi, H. Vinh-Thang, S. Mikhailenko, S. Kaliaguine, *J. Power Sources* **2013**, *239*, 415.
[54] J. Ying, G. Jiang, Z. Paul Cano, L. Han, X.-Y. Yang, Z. Chen, *Nano Energy* **2017**, *40*, 88.
[55] J. Ying, J. Li, G. Jiang, Z. P. Cano, Z. Ma, C. Zhong, D. Su, Z. Chen, *Appl. Catal. B* **2018**, *225*, 496.
[56] I. C. Gerber, P. Serp, *Chem. Rev.* **2020**, *120*, 1250.
[57] J. Wang, J. Kim, S. Choi, H. Wang, J. Lim, *Small Methods* **2020**, *4*, 2000621.
[58] G. Wu, K. L. More, C. M. Johnston, P. Zelenay, *Science* **2011**, *332*, 443.
[59] Z. S. Wu, L. Chen, J. Liu, K. Parvez, H. Liang, J. Shu, H. Sachdev, R. Graf, X. Feng, K. Mullen, *Adv. Mater.* **2014**, *26*, 1450.
[60] S. H. Noh, M. H. Seo, X. Ye, Y. Makinose, T. Okajima, N. Matsushita, B. Han, T. Ohsaka, *J. Mater. Chem. A* **2015**, *3*, 22031.
[61] J. Wang, H. Wu, D. Gao, S. Miao, G. Wang, X. Bao, *Nano Energy* **2015**, *13*, 387.
[62] G. Zhang, G. Wang, Y. Liu, H. Liu, J. Qu, J. Li, *J. Am. Chem. Soc.* **2016**, *138*, 14686.
[63] Y. Zhou, R. Ma, P. Li, Y. Chen, Q. Liu, G. Cao, J. Wang, *J. Mater. Chem. A* **2016**, *4*, 8204.
[64] L. Ai, T. Tian, J. Jiang, *ACS Sustainable Chem. Eng.* **2017**, *5*, 4771.
[65] Y. Chen, S. Xu, S. Zhu, R. J. Jacob, G. Pastel, Y. Wang, Y. Li, J. Dai, F. Chen, H. Xie, B. Liu, Y. Yao, L. G. Salamanca-Riba, M. R. Zachariah, T. Li, L. Hu, *Nano Res.* **2019**, *12*, 2259.
[66] J. Cao, K. Wang, J. Chen, C. Lei, B. Yang, Z. Li, L. Lei, Y. Hou, K. Ostrikov, *Nano-Micro Lett.* **2019**, *11*, 67.
[67] H. Jin, X. Wang, C. Tang, A. Vasileff, L. Li, A. Slattery, S. Z. Qiao, *Adv. Mater.* **2021**, *33*, 2007508.
[68] J. Li, Y. Wang, T. Zhou, H. Zhang, X. Sun, J. Tang, L. Zhang, A. M. Al-Enizi, Z. Yang, G. Zheng, *J. Am. Chem. Soc.* **2015**, *137*, 14305.
[69] J. Su, G. Xia, R. Li, Y. Yang, J. Chen, R. Shi, P. Jiang, Q. Chen, *J. Mater. Chem. A* **2016**, *4*, 9204.
[70] J. Deng, D. Deng, X. Bao, *Adv. Mater.* **2017**, *29*, 1606967.
[71] B. Ni, L. Wu, R. Chen, C. Shi, T. Chen, *Sci. China Mater.* **2019**, *62*, 1626.
[72] Y. Peng, S. Chen, *Green Energy Environ.* **2018**, *3*, 335.
[73] A. B. Grommet, M. Feller, R. Klajn, *Nat. Nanotechnol.* **2020**, *15*, 256.
[74] D. Thanh Tran, T. Kshetri, N. Dinh Chuong, J. Gautam, H. Van Hien, L. Huu Tuan, N. H. Kim, J. H. Lee, *Nano Today* **2018**, *22*, 100.
[75] L. Tang, X. Meng, D. Deng, X. Bao, *Adv. Mater.* **2019**, *31*, 1901996.
[76] Z. P. Wu, X. F. Lu, S. Q. Zang, X. W. Lou, *Adv. Funct. Mater.* **2020**, *30*, 1910274.
[77] B. Zhang, Y. Zheng, T. Ma, C. Yang, Y. Peng, Z. Zhou, M. Zhou, S. Li, Y. Wang, C. Cheng, *Adv. Mater.* **2021**, *33*, 2006042.
[78] M. Tavakkoli, T. Kallio, O. Reynaud, A. G. Nasibulin, C. Johans, J. Sainio, H. Jiang, E. I. Kauppinen, K. Laasonen, *Angew. Chem., Int. Ed.* **2015**, *54*, 4535.
[79] H. Zhang, Z. Ma, J. Duan, H. Liu, G. Liu, T. Wang, K. Chang, M. Li, L. Shi, X. Meng, K. Wu, J. Ye, *ACS Nano* **2016**, *10*, 684.
[80] Y. Wang, Y. Nie, W. Ding, S. G. Chen, K. Xiong, X. Q. Qi, Y. Zhang, J. Wang, Z. D. Wei, *Chem. Commun.* **2015**, *51*, 8942.
[81] J. Liu, L. Xu, Y. Deng, X. Zhu, J. Deng, J. Lian, J. Wu, J. Qian, H. Xu, S. Yuan, H. Li, P. M. Ajayan, *J. Mater. Chem. A* **2019**, *7*, 14291.
[82] J. Mahmood, F. Li, C. Kim, H.-J. Choi, O. Gwon, S.-M. Jung, J.-M. Seo, S.-J. Cho, Y.-W. Ju, H. Y. Jeong, G. Kim, J.-B. Baek, *Nano Energy* **2018**, *44*, 304.
[83] M. Sharma, J.-H. Jang, D. Y. Shin, J. A. Kwon, D.-H. Lim, D. Choi, H. Sung, J. Jang, S.-Y. Lee, K. Y. Lee, H.-Y. Park, N. Jung, S. J. Yoo, *Energy Environ. Sci.* **2019**, *12*, 2200.
[84] W. Yang, L. Chen, X. Liu, J. Jia, S. Guo, *Nanoscale* **2017**, *9*, 1738.
[85] Y. Li, F. Cheng, J. Zhang, Z. Chen, Q. Xu, S. Guo, *Small* **2016**, *12*, 2839.
[86] E. Hu, J. Ning, B. He, Z. Li, C. Zheng, Y. Zhong, Z. Zhang, Y. Hu, *J. Mater. Chem. A* **2017**, *5*, 2271.
[87] X. Zhang, J. Lin, S. Chen, J. Yang, L. Song, X. Wu, H. Xu, *ACS Appl. Mater. Interfaces* **2017**, *9*, 38499.
[88] Y. Zhao, J. Zhang, K. Li, Z. Ao, C. Wang, H. Liu, K. Sun, G. Wang, *J. Mater. Chem. A* **2016**, *4*, 12818.
[89] Y. Yang, Z. Lun, G. Xia, F. Zheng, M. He, Q. Chen, *Energy Environ. Sci.* **2015**, *8*, 3563.
[90] Z. Pu, I. S. Amiinu, C. Zhang, M. Wang, Z. Kou, S. Mu, *Nanoscale* **2017**, *9*, 3555.
[91] J. Deng, P. Ren, D. Deng, X. Bao, *Angew. Chem., Int. Ed.* **2015**, *54*, 2100.
[92] M. Zhuang, X. Ou, Y. Dou, L. Zhang, Q. Zhang, R. Wu, Y. Ding, M. Shao, Z. Luo, *Nano Lett.* **2016**, *16*, 4691.
[93] K. Hu, T. Ohto, L. Chen, J. Han, M. Wakisaka, Y. Nagata, J.-I. Fujita, Y. Ito, *ACS Energy Lett.* **2018**, *3*, 1539.
[94] M. Miao, R. Hou, Z. Liang, R. Qi, T. He, Y. Yan, K. Qi, H. Liu, G. Feng, B. Y. Xia, *J. Mater. Chem. A* **2018**, *6*, 24107.
[95] R. Wang, X. Y. Dong, J. Du, J. Y. Zhao, S. Q. Zang, *Adv. Mater.* **2018**, *30*, 1703711.
[96] Y. Liu, G. Yu, G. D. Li, Y. Sun, T. Asefa, W. Chen, X. Zou, *Angew. Chem., Int. Ed.* **2015**, *54*, 10752.
[97] R. Ma, Y. Zhou, Y. Chen, P. Li, Q. Liu, J. Wang, *Angew. Chem., Int. Ed.* **2015**, *54*, 14723.
[98] Z. Pu, I. S. Amiinu, X. Liu, M. Wang, S. Mu, *Nanoscale* **2016**, *8*, 17256.
[99] Z. Pu, X. Ya, I. S. Amiinu, Z. Tu, X. Liu, W. Li, S. Mu, *J. Mater. Chem. A* **2016**, *4*, 15327.
[100] Y.-Y. Ma, C.-X. Wu, X.-J. Feng, H.-Q. Tan, L.-K. Yan, Y. Liu, Z.-H. Kang, E.-B. Wang, Y.-G. Li, *Energy Environ. Sci.* **2017**, *10*, 788.
[101] Y. Yang, Z. Lin, S. Gao, J. Su, Z. Lun, G. Xia, J. Chen, R. Zhang, Q. Chen, *ACS Catal.* **2017**, *7*, 469.
[102] Y. Gu, S. Chen, J. Ren, Y. A. Jia, C. Chen, S. Komarneni, D. Yang, X. Yao, *ACS Nano* **2018**, *12*, 245.
[103] L. Liu, X. Yang, N. Ma, H. Liu, Y. Xia, C. Chen, D. Yang, X. Yao, *Small* **2016**, *12*, 1295.
[104] D. Xie, Y. Chen, D. Yu, S. Han, J. Song, Y. Xie, F. Hu, L. Li, S. Peng, *Chem. Commun.* **2020**, *56*, 6842.
[105] N. Wu, Y. Lei, Q. Wang, B. Wang, C. Han, Y. Wang, *Nano Res.* **2017**, *10*, 2332.
[106] J. Zhu, M. Xiao, Y. Zhang, Z. Jin, Z. Peng, C. Liu, S. Chen, J. Ge, W. Xing, *ACS Catal.* **2016**, *6*, 6335.
[107] Z. Wang, X. Liao, Z. Lin, F. Huang, Y. Jiang, K. A. Owusu, L. Xu, Z. Liu, J. Li, Y. Zhao, Y. B. Cheng, L. Mai, *Chem. - Eur. J.* **2020**, *26*, 4044.
[108] Y. Liang, Y. Li, H. Wang, J. Zhou, J. Wang, T. Regier, H. Dai, *Nat. Mater.* **2011**, *10*, 780.
[109] D. Zhao, Q. Shao, Y. Zhang, X. Huang, *Nanoscale* **2018**, *10*, 22787.
[110] Y. Tu, P. Ren, D. Deng, X. Bao, *Nano Energy* **2018**, *52*, 494.
[111] X. Cui, P. Ren, D. Deng, J. Deng, X. Bao, *Energy Environ. Sci.* **2016**, *9*, 123.
[112] F. Yu, Y. Gao, Z. Lang, Y. Ma, L. Yin, J. Du, H. Tan, Y. Wang, Y. Li, *Nanoscale* **2018**, *10*, 6080.
[113] W. Xiao, L. Zhang, D. Bukhvalov, Z. Chen, Z. Zou, L. Shang, X. Yang, D. Yan, F. Han, T. Zhang, *Nano Energy* **2020**, *70*, 104445.
[114] T. Wang, Q. Zhou, X. Wang, J. Zheng, X. Li, *J. Mater. Chem. A* **2015**, *3*, 16435.

[115] A. Majeed, X. Li, P.-X. Hou, H. Tabassum, L. Zhang, C. Liu, H.-M. Cheng, *Appl. Catal., B* **2020**, *269*, 118823.
[116] Z. Wang, H. Jin, T. Meng, K. Liao, W. Meng, J. Yang, D. He, Y. Xiong, S. Mu, *Adv. Funct. Mater.* **2018**, *28*, 1802596.
[117] J. Ryu, N. Jung, D. H. Lim, D. Y. Shin, S. H. Park, H. C. Ham, J. H. Jang, H. J. Kim, S. J. Yoo, *Chem. Commun.* **2014**, *50*, 15940.
[118] Q. Zhang, P. Kumar, X. Zhu, R. Daiyan, N. M. Bedford, K. H. Wu, Z. Han, T. Zhang, R. Amal, X. Lu, *Adv. Energy Mater.* **2021**, *11*, 2100303.
[119] W. Zhang, W. Chen, Q. Xiao, L. Yu, C. Huang, G. Lu, A. W. Morawski, Y. Yu, *Appl. Catal., B* **2020**, *268*, 118449.
[120] X. Lv, J. Ren, Y. Wang, Y. Liu, Z.-Y. Yuan, *ACS Sustainable Chem. Eng.* **2019**, *7*, 8993.
[121] X. Liu, W. Li, X. Zhao, Y. Liu, C. W. Nan, L. Z. Fan, *Adv. Funct. Mater.* **2019**, *29*, 1901510.
[122] L. N. Zhang, S. H. Li, H. Q. Tan, S. U. Khan, Y. Y. Ma, H. Y. Zang, Y. H. Wang, Y. G. Li, *ACS Appl. Mater. Interfaces* **2017**, *9*, 16270.
[123] Z. Yu, Y. Bai, S. Zhang, Y. Liu, N. Zhang, G. Wang, J. Wei, Q. Wu, K. Sun, *ACS Appl. Mater. Interfaces* **2018**, *10*, 6245.
[124] J. Yang, D. Guo, S. Zhao, Y. Lin, R. Yang, D. Xu, N. Shi, X. Zhang, L. Lu, Y. Q. Lan, J. Bao, M. Han, *Small* **2019**, *15*, 1804546.
[125] E. Hu, X.-Y. Yu, F. Chen, Y. Wu, Y. Hu, X. W. D. Lou, *Adv. Energy Mater.* **2018**, *8*, 1702476.
[126] X. Zhong, Y. Jiang, X. Chen, L. Wang, G. Zhuang, X. Li, J.-G. Wang, *J. Mater. Chem. A* **2016**, *4*, 10575.
[127] Z. Pu, C. Zhang, I. S. Amiinu, W. Li, L. Wu, S. Mu, *ACS Appl. Mater. Interfaces* **2017**, *9*, 16187.
[128] H. Khani, N. S. Grundish, D. O. Wipf, J. B. Goodenough, *Adv. Energy Mater.* **2019**, *10*, 1903215.
[129] J. Wang, G. Wang, S. Miao, J. Li, X. Bao, *Faraday Discuss.* **2014**, *176*, 135.
[130] D. Zhao, K. Sun, W. C. Cheong, L. Zheng, C. Zhang, S. Liu, X. Cao, K. Wu, Y. Pan, Z. Zhuang, B. Hu, D. Wang, Q. Peng, C. Chen, Y. Li, *Angew. Chem., Int. Ed.* **2020**, *59*, 8982.
[131] S. Dang, Q.-L. Zhu, Q. Xu, *Nat. Rev. Mater.* **2017**, *3*, 17075.
[132] Z. H. Zhu, B. H. Zhao, S. L. Hou, X. L. Jiang, Z. L. Liang, B. Zhang, B. Zhao, *Angew. Chem., Int. Ed.* **2021**, 60, 23394 .
[133] D. Ren, J. Ying, M. Xiao, Y. P. Deng, J. Ou, J. Zhu, G. Liu, Y. Pei, S. Li, A. M. Jauhar, H. Jin, S. Wang, D. Su, A. Yu, Z. Chen, *Adv. Funct. Mater.* **2019**, *30*, 1908167.
[134] Y. Tian, L. Xu, J. Bao, J. Qian, H. Su, H. Li, H. Gu, C. Yan, H. Li, *J. Energy Chem.* **2019**, *33*, 59.
[135] D. Wu, C. Zhu, Y. Shi, H. Jing, J. Hu, X. Song, D. Si, S. Liang, C. Hao, *ACS Sustainable Chem. Eng.* **2018**, *7*, 1137.
[136] L. Li, G. Zhang, Z. Su, *Angew. Chem., Int. Ed.* **2016**, *55*, 9093.
[137] Y. Yang, X. Liang, F. Li, S. Li, X. Li, S. P. Ng, C. L. Wu, R. Li, *ChemSusChem* **2018**, *11*, 376.
[138] F. Shen, W. Jiang, G. Qian, W. Chen, H. Zhang, L. Luo, S. Yin, *J. Power Sources* **2020**, *458*, 228014.
[139] K. Choy, *Prog. Mater. Sci.* **2003**, *48*, 57.
[140] P. Marchand, I. A. Hassan, I. P. Parkin, C. J. Carmalt, *Dalton Trans.* **2013**, *42*, 9406.
[141] P. Trogadas, V. Ramani, P. Strasser, T. F. Fuller, M. O. Coppens, *Angew. Chem., Int. Ed.* **2016**, *55*, 122.
[142] X. Fan, Z. Peng, R. Ye, H. Zhou, X. Guo, *ACS Nano* **2015**, *9*, 7407.
[143] J. Wang, X. Cui, H. Li, J. Xiao, J. Yang, X. Mu, H. Liu, Y.-M. Sun, X. Xue, C. Liu, X.-D. Zhang, D. Deng, X. Bao, *Nano Res.* **2018**, *11*, 2821.
[144] H. Fei, Y. Yang, Z. Peng, G. Ruan, Q. Zhong, L. Li, E. L. Samuel, J. M. Tour, *ACS Appl. Mater. Interfaces* **2015**, *7*, 8083.
[145] Y. Shen, Y. Zhou, D. Wang, X. Wu, J. Li, J. Xi, *Adv. Energy Mater.* **2018**, *8*, 1701759.
[146] X. Zou, X. Huang, A. Goswami, R. Silva, B. R. Sathe, E. Mikmekova, T. Asefa, *Angew. Chem., Int. Ed.* **2014**, *53*, 4372.
[147] D. Deng, K. S. Novoselov, Q. Fu, N. Zheng, Z. Tian, X. Bao, *Nat. Nanotechnol.* **2016**, *11*, 218.
[148] S. M. Wu, X. Y. Yang, C. Janiak, *Angew. Chem., Int. Ed.* **2019**, *58*, 12340.
[149] L.-P. Yuan, T. Tang, J.-S. Hu, L.-J. Wan, *Acc. Mater. Res.* **2021**, 10, 907.
[150] S. Wang, X. Huang, Y. He, H. Huang, Y. Wu, L. Hou, X. Liu, T. Yang, J. Zou, B. Huang, *Carbon* **2012**, *50*, 2119.
[151] J. Wang, D. Gao, G. Wang, S. Miao, H. Wu, J. Li, X. Bao, *J. Mater. Chem. A* **2014**, *2*, 20067.
[152] S. Gao, G. D. Li, Y. Liu, H. Chen, L. L. Feng, Y. Wang, M. Yang, D. Wang, S. Wang, X. Zou, *Nanoscale* **2015**, *7*, 2306.
[153] L. Yu, D. Deng, X. Bao, *Angew. Chem., Int. Ed.* **2020**, *59*, 15294.
[154] C. K. Yang, J. Zhao, J. P. Lu, *Phys. Rev. Lett.* **2003**, *90*, 257203.
[155] F. Guinea, *Phys. Rev. B* **2007**, *75*, 235433.
[156] Y. Xie, J. M. Zhang, Y. P. Huo, *Eur. Phys. J. B* **2011**, *81*, 459.
[157] K. Strickland, E. Miner, Q. Jia, U. Tylus, N. Ramaswamy, W. Liang, M. T. Sougrati, F. Jaouen, S. Mukerjee, *Nat. Commun.* **2015**, *6*, 7343.
[158] W. Zhou, J. Zhou, Y. Zhou, J. Lu, K. Zhou, L. Yang, Z. Tang, L. Li, S. Chen, *Chem. Mater.* **2015**, *27*, 2026.
[159] S. Zhu, M. Shao, *J. Solid State Electrochem.* **2015**, *20*, 861.
[160] D. Deng, L. Yu, X. Chen, G. Wang, L. Jin, X. Pan, J. Deng, G. Sun, X. Bao, *Angew. Chem., Int. Ed.* **2013**, *52*, 371.
[161] J. Deng, L. Yu, D. Deng, X. Chen, F. Yang, X. Bao, *J. Mater. Chem. A* **2013**, *1*, 14868.
[162] J. Duan, S. Chen, M. Jaroniec, S. Z. Qiao, *ACS Catal.* **2015**, *5*, 5207.
[163] Y. Zheng, Y. Jiao, L. Ge, M. Jaroniec, S. Z. Qiao, *Angew. Chem., Int. Ed.* **2013**, *52*, 3110.
[164] M. Antonietti, N. Lopez-Salas, A. Primo, *Adv. Mater.* **2019**, *31*, 1805719.
[165] R. Parsons, *Trans. Faraday Soc.* **1958**, *54*, 1053.
[166] R. Wu, J. Zhang, Y. Shi, D. Liu, B. Zhang, *J. Am. Chem. Soc.* **2015**, *137*, 6983.
[167] Z. Chen, R. Wu, Y. Liu, Y. Ha, Y. Guo, D. Sun, M. Liu, F. Fang, *Adv. Mater.* **2018**, *30*, 1802011.
[168] Z. Zhen, Z. Jiang, X. Tian, L. Zhou, B. Deng, B. Chen, Z.-J. Jiang, *RSC Adv.* **2018**, *8*, 14462.
[169] P. C. Chen, X. Liu, J. L. Hedrick, Z. Xie, S. Wang, Q. Y. Lin, M. C. Hersam, V. P. Dravid, C. A. Mirkin, *Science* **2016**, *352*, 1565.
[170] Y. Wang, H. Z. Yu, J. Ying, G. Tian, Y. Liu, W. Geng, J. Hu, Y. Lu, G. G. Chang, K. I. Ozoemena, C. Janiak, X. Y. Yang, *Chem. - Eur. J.* **2021**, *27*, 9124.
[171] Y. X. Xiao, J. Ying, G. Tian, X. Yang, Y. X. Zhang, J. B. Chen, Y. Wang, M. D. Symes, K. I. Ozoemena, J. Wu, X. Y. Yang, *Nano Lett.* **2021**, 21, 7870.
[172] P. Strasser, S. Koh, T. Anniyev, J. Greeley, K. More, C. Yu, Z. Liu, S. Kaya, D. Nordlund, H. Ogasawara, M. F. Toney, A. Nilsson, *Nat. Chem.* **2010**, *2*, 454.
[173] J. Li, S. Sun, *Acc. Chem. Res.* **2019**, *52*, 2015.
[174] V. Ponec, *Appl. Catal. A* **2001**, *222*, 31.
[175] J. R. Kitchin, J. K. Norskov, M. A. Barteau, J. G. Chen, *Phys. Rev. Lett.* **2004**, *93*, 156801.
[176] Y. Zheng, Y. Jiao, M. Jaroniec, S. Z. Qiao, *Angew. Chem., Int. Ed.* **2015**, *54*, 52.
[177] I. C. Man, H. Y. Su, F. Calle-Vallejo, H. A. Hansen, J. I. Martínez, N. G. Inoglu, J. Kitchin, T. F. Jaramillo, J. K. Nørskov, J. Rossmeisl, *ChemCatChem* **2011**, *3*, 1159.
[178] O. Mashtalir, M. Naguib, V. N. Mochalin, Y. Dall'Agnese, M. Heon, M. W. Barsoum, Y. Gogotsi, *Nat. Commun.* **2013**, *4*, 1716.
[179] Y. Xie, M. Naguib, V. N. Mochalin, M. W. Barsoum, Y. Gogotsi, X. Yu, K. W. Nam, X. Q. Yang, A. I. Kolesnikov, P. R. Kent, *J. Am. Chem. Soc.* **2014**, *136*, 6385.
[180] C. Wan, B. M. Leonard, *Chem. Mater.* **2015**, *27*, 4281.
[181] J. Yin, Q. Fan, Y. Li, F. Cheng, P. Zhou, P. Xi, S. Sun, *J. Am. Chem. Soc.* **2016**, *138*, 14546.
[182] H. Lin, N. Liu, Z. Shi, Y. Guo, Y. Tang, Q. Gao, *Adv. Funct. Mater.* **2016**, *26*, 5590.
[183] K. Xiong, L. Li, L. Zhang, W. Ding, L. Peng, Y. Wang, S. Chen, S. Tan, Z. Wei, *J. Mater. Chem. A* **2015**, *3*, 1863.

[184] S. Wang, L. Pan, J. J. Song, W. Mi, J. J. Zou, L. Wang, X. Zhang, *J. Am. Chem. Soc.* **2015**, *137*, 2975.
[185] T. C. Schulthess, W. M. Temmerman, Z. Szotek, W. H. Butler, G. M. Stocks, *Nat. Mater.* **2005**, *4*, 838.
[186] C. Lin, X. Zhu, J. Feng, C. Wu, S. Hu, J. Peng, Y. Guo, L. Peng, J. Zhao, J. Huang, J. Yang, Y. Xie, *J. Am. Chem. Soc.* **2013**, *135*, 5144.
[187] J. Low, J. Yu, M. Jaroniec, S. Wageh, A. A. Al-Ghamdi, *Adv. Mater.* **2017**, *29*, 1601694.
[188] J. Su, G. D. Li, X. H. Li, J. S. Chen, *Adv. Sci.* **2019**, *6*, 1801702.
[189] H. Z. Yu, Y. Wang, J. Ying, S. M. Wu, Y. Lu, J. Hu, J. S. Hu, L. Shen, Y. X. Xiao, W. Geng, G. G. Chang, C. Janiak, W. H. Li, X. Y. Yang, *ACS Appl. Mater. Interfaces* **2019**, *11*, 27641.
[190] Z. Wen, S. Ci, F. Zhang, X. Feng, S. Cui, S. Mao, S. Luo, Z. He, J. Chen, *Adv. Mater.* **2012**, *24*, 1399.
[191] Y. Lu, X. Cheng, G. Tian, H. Zhao, L. He, J. Hu, S.-M. Wu, Y. Dong, G.-G. Chang, S. Lenaerts, S. Siffert, G. Van Tendeloo, Z.-F. Li, L.-L. Xu, X.-Y. Yang, B.-L. Su, *Nano Energy* **2018**, *47*, 8.
[192] Y. Dong, S. Y. Chen, Y. Lu, Y. X. Xiao, J. Hu, S. M. Wu, Z. Deng, G. Tian, G. G. Chang, J. Li, S. Lenaerts, C. Janiak, X. Y. Yang, B. L. Su, *Chem. Asian J.* **2018**, *13*, 1609.
[193] T. Dong, X. Zhang, Y. Cao, H.-S. Chen, P. Yang, *Inorg. Chem. Front.* **2019**, *6*, 1073.
[194] P. Ji, H. Jin, H. Xia, X. Luo, J. Zhu, Z. Pu, S. Mu, *ACS Appl. Mater. Interfaces* **2020**, *12*, 727.
[195] Y. Lu, X. L. Liu, L. He, Y. X. Zhang, Z. Y. Hu, G. Tian, X. Cheng, S. M. Wu, Y. Z. Li, X. H. Yang, L. Y. Wang, J. W. Liu, C. Janiak, G. G. Chang, W. H. Li, G. Van Tendeloo, X. Y. Yang, B. L. Su, *Nano Lett.* **2020**, *20*, 3122.
[196] S. Zhao, M. Li, M. Han, D. Xu, J. Yang, Y. Lin, N.-E. Shi, Y. Lu, R. Yang, B. Liu, Z. Dai, J. Bao, *Adv. Funct. Mater.* **2018**, *28*, 1706018.
[197] Y. Tu, J. Deng, C. Ma, L. Yu, X. Bao, D. Deng, *Nano Energy* **2020**, *72*, 104700.
[198] J. Chen, Y. Bai, J. Feng, F. Yang, P. Xu, Z. Wang, Q. Zhang, Y. Yin, *Angew. Chem., Int. Ed.* **2021**, *60*, 4117.
[199] E. P. George, D. Raabe, R. O. Ritchie, *Nat. Rev. Mater.* **2019**, *4*, 515.
[200] Y. Yao, Z. Huang, P. Xie, S. D. Lacey, R. J. Jacob, H. Xie, F. Chen, A. Nie, T. Pu, M. Rehwoldt, D. Yu, M. R. Zachariah, C. Wang, R. Shahbazian-Yassar, J. Li, L. Hu, *Science* **2018**, *359*, 1489.
[201] T. Li, Y. Yao, Z. Huang, P. Xie, Z. Liu, M. Yang, J. Gao, K. Zeng, A. H. Brozena, G. Pastel, M. Jiao, Q. Dong, J. Dai, S. Li, H. Zong, M. Chi, J. Luo, Y. Mo, G. Wang, C. Wang, R. Shahbazian-Yassar, L. Hu, *Nat. Catal.* **2021**, *4*, 62.
[202] Y. Yao, Z. Huang, L. A. Hughes, J. Gao, T. Li, D. Morris, S. E. Zeltmann, B. H. Savitzky, C. Ophus, Y. Z. Finfrock, Q. Dong, M. Jiao, Y. Mao, M. Chi, P. Zhang, J. Li, A. M. Minor, R. Shahbazian-Yassar, L. Hu, *Matter* **2021**, *4*, 2340.
[203] M. Tang, W. Yuan, Y. Ou, G. Li, R. You, S. Li, H. Yang, Z. Zhang, Y. Wang, *ACS Catal.* **2020**, *10*, 14419.
[204] J. Li, J. Gong, *Energy Environ. Sci.* **2020**, *13*, 3748.
[205] Y. Zhu, T.-R. Kuo, Y.-H. Li, M.-Y. Qi, G. Chen, J. Wang, Y.-J. Xu, H. M. Chen, *Energy Environ. Sci.* **2021**, *14*, 1928.
[206] G. Rupprechter, *Small* **2021**, *17*, 2004289.

Ling Shen received his bachelor's degree from Wuhan University of technology in 2014. Currently, he is a Ph.D. candidate at School of Materials Science and Engineering, Wuhan University of Technology (WUT). His current research focuses on the design, synthesis, and applications of carbon-based materials.

Jie Ying received his Ph.D. degree from Wuhan University of Technology in 2016. He then joined the group of Prof. Zhongwei Chen at the University of Waterloo (2016) and Prof. Christoph Janiak at Heinrich-Heine-Universität Düsseldorf (2018) as a postdoctoral fellow. Currently, he is an associate professor in Sun Yat-sen University. His scientific interest includes design and synthesis of nanocomposite and their application in catalysis and electrocatalysis.

Kenneth I. Ozoemena is a professor of Materials for Energy & Electrochemistry at the University of the Witwatersrand (Wits), South Africa. Prior to joining Wits in 2017, he had worked at the South Africa's Council for Scientific and Industrial Research as Chief Research Scientist and Research Group Leader of the CSIR Electrochemical Energy Technologies (2009–2017). His current research interests are focused on energy storage and conversion systems and electrochemical sensors.

Christoph Janiak is a full professor for Nanoporous and Nanoscale Materials at the University of Düsseldorf since 2010, with research interests in the synthesis and properties of metal-organic frameworks (MOFs) and porous organic polymers, mixed-matrix membranes, metal nanoparticles, ionic liquids, and catalysis. Until 2018 he was a visiting professor at Wuhan University of Technology and currently he is a guest professor at the Hoffmann Institute of Advanced Materials at Shenzhen Polytechnic in China.

Xiao-Yu Yang received his Ph.D. from Jilin University (coeducated at FUNDP of Belgium). After a postdoctoral fellowship at the FUNDP, he worked as a "Chargé de Recherches" at the FNRS in Belgium. He is currently working as a full professor at WUT, coprofessor at SMSEGL and SYSU, and visiting professor at HU. His research is aimed at hierarchical assembly techniques and hierarchical structured materials for the applications in energy, environment, catalysis, bioengineering, and ocean engineering.